DOGUS UNIVERSITY

INSTITUTE OF SCIENCE AND TECHNOLOGY

DEPARTMENT OF ELECTRONICS AND COMMUNICATIONS ENGINEERING

METHOD OF MOMENT MODELING OF WAVE SCATTERING FROM ARBITRARY GEOMETRIES IN 3-D IN FREE SPACE

M.Sc. THESIS

Ahmet SEFER

201192001

Thesis Advisor: Prof. Dr. Levent SEVGI

Dogus University, June 2014

DOGUS UNIVERSITY

INSTITUTE OF SCIENCE AND TECHNOLOGY

DEPARTMENT OF ELECTRONICS AND COMMUNICATION ENGINEERING

METHOD OF MOMENT MODELING OF WAVE SCATTERING FROM ARBITRARY GEOMETRIES IN 3-D IN FREE SPACE

M.Sc. THESIS

Ahmet SEFER

201192001

Thesis Advisor: Prof. Dr. Levent SEVGI

Dogus University, June 2014

T.C. DOĞUŞ ÜNİVERSİTESİ

FEN BİLİMLERİ ENSTİTÜSÜ

ELEKTRONİK HABERLEŞME MÜHENDİSLİĞİ ANABİLİM DALI

BOŞ UZAYDA 3 BOYUTLU RASTGELE SEÇİLMİŞ GEOMETRİLER İÇİN DALGA SAÇILMASININ MOMENT YÖNTEMI İLE MODELLEMESİ

Bitirme Tezi

Ahmet SEFER

201192001

Tez Danışmanı: Prof. Dr. Levent SEVGİ

Doğuş Üniversitesi, Haziran 2014

To her, my beloved Zeynep,

Foreword

I would like to thank to the following esteemed academicians, who have had great impact on my thesis. First, I would like many thanks to my supervisor, Professor Levent Sevgi, for not only for his valuable insights and patient guidance to complete the research; but also his standing as an academician which always inspires to me. Without his efforts, this thesis would not be a success. Then, many thanks to Professor Ercan Topuz who is always open to help whenever I needed with his great knowledge on electromagnetic theory. Third, many thanks to Professor Cem Göknar, from whom I have learned how to ask the "right" questions. Lastly, many thanks to Assistant Professor Dilek B. Tukel and Associate Professor Mustafa Doğan for their precious concerns and great encouragements to me.

Besides, I would like to thanks to my family and two special people, Ahmet Aydoğan and Dalga Teoman, my friends, and my colleagues, for all their valuable supports.

Last, but no means least, I would like to thank Zeynep, my beloved, for her patience, supports and her confidence to me.

Istanbul, June 2014 Ahmet SEFER

TABLE OF CONTENTS

ABBREVIATIONS

EM: Electromagnetic

MoM: Method of Moments

FDTD: Finite Different Time Domain

VIE: Volume Integral Equation

SIE: Surface Integral Equation

EFIE: Electric Field Integral Equation

PEC: Perfectly Electrical Conducting

PV: Principle Value

GO: Geometric Optics

RCS: Radar Cross Section

RSY: Radar Saçılma Yüzeyi

MY: Moment Yöntemi

LIST OF FIGURES

LIST OF TABLES

SUMMARY

In this thesis, wave scattering from electromagnetic (EM) wave – object interaction and radar cross section (RCS) prediction of arbitrary-shaped (conducting or dielectric) objects in three dimensional (3-D) free space is considered. Problem is formulated in terms of volume integral equations containing Dyadic Green Functions. Method of Moments (MoM) is used to the given problem. In the context of MoM, point matching technique is applied. The volume of the scatterer is represented by cubical cells over which the electric field is assumed constant. The electric field integral equation (EFIE) is enforced at the center of each cell to produce a system of equations in a matrix form. Here, the incident field, location, geometry and electrical parameters (relative permittivity and conductivity of the object) of the object are known. The unknowns are the equivalent volume current densities. After obtaining the unknowns of the problem, one can easily derive scattered fields at any given point in the space. This is then used in RCS calculations for both bistatic and monostatic cases.

The algorithm developed for this purpose is coded in MATLAB. The model and the algorithm are already validated; here only the code is verified through some canonical tests and comparisons. First, a reference object – sphere – is used. The sphere has analytical exact solution in terms of Mie series summation. Another MATLAB code is prepared for the accurate calculation of the analytical solution. To be able to acquire satisfactory results for a sphere, the size of the cells are smaller than $\lambda/50$ which depends also the values of relative permittivity. Simulations are performed for different material spheres. Simulations of perfectly electrical conducting (PEC) canonical structures are also performed and results are compared with the Transient Solver code of CST Microwave Studio which uses Finite Difference Time Domain.

ÖZET

Bu çalışmada, üç boyutlu boş uzaya yerleştirilmiş,–iletken veya kayıplı yalıtkan- bir cisim üzerinde ki elektromanyetik etkileşimler ve bu cisim için Radar Saçılma Yüzeyi (RSY) hesaplamaları ele alınmıştır. Problem, diyadik Green Fonksiyonlarını içeren hacim integral denklemleri ile formüle edilmiştir. Elde edilen denklemlerin lineer formda çözümü için Moment Yöntemine (MY) başvurulmuştur. Bu bağlamda, elektromanyetik saçılmanın gözlemleneceği cismin hacmi küçük kübik hücreler ile ayrıklaştırılır ve bu hücrelerin üzerinde ki elektrik alanların sabit olduğu kabul edilir. Her bir kübik hacmin ortası için elektrik alan integral denklemlerine başvurularak, sistem için oluşturulan denklem matris formuna ulaşılır. Matris formunda elde edilen bu denklemler için, cisme gelen alan, cismin konumu, geometrisi ve elektriksel parametreleri bilinen parametrelerdir. Bulunmak istenilen ise, kübik hacimler üzerinde ki eşdeğer akımlardır. Matris denklemlerinin çözümü ile bu akımlar elde edildikten sonra, uzayda ki herhangi bir nokta için saçılan elektromanyetik alanları elde etmek mümkündür. Böylelikle, cisimden saçılan alanların uzayda belirli gözlem bölgelerini içeren monostatik ve bistatik RSY hesaplamaları yapmak mümkün olabilmektedir.

Yukarıda bahsedilen algoritma MATLAB tabanlı kod yazılarak oluşturulmuştur. Oluşturulan kodun doğrulaması, birtakım kanonik testler ve kıyaslamalar ile yapılmıştır. Öncelikle, Mie serilerine başvurularak, analitik olarak çözülmesi mümkün olan küre, sayısal algoritmanın doğruluğunu test etmek amacıyla, referans cisim olarak ele alınmıştır. Bu bağlamda, küre için analitik çözümlemelerde başvurulacak bir diğer MATLAB tabanlı kod da hazırlanmıştır. Sayısal ve analitik yöntemlerin kıyaslanması için birçok farklı malzemeden elde edilmiş küresel cismin simülasyonu yapılmıştır. MY ile küreden saçılan alanların hesaplanmasında, çoğu simülasyon sonunda, tatmin edici sonuçlar elde edebilmek için, kübik hücrelerin boyutları, seçilen frekansta ki dalga boyunun ellide birinden daha küçük boyutlarda modellenmek zorunda kalınmıştır. Elektriksel olarak mükemmel iletken olan diğer kanonik yapılar içinde simülasyonlar yapılmış; eş zamanlı olarak, ticari bir elektromanyetik simülasyon programı olan ve elektromanyetik hesaplamalar için bir diğer sayısal yöntem, Zaman Domeninde Sonlu farklar (FDTD) kullanan,

CST Microwave - Transient Solver ile bahsedilen kanonik cisimlerin simülasyonları yapılıp; elde edilen sonuçlar ile kıyaslanmıştır.

1. INTRODUCTION

Electromagnetic wave scattering has been investigated for nearly a century. The scattering characteristics are represented via the radar cross section (RCS) of an object. Early studies belong to high frequencies where wavelength is much smaller than the size of the object under investigation. In this case, it is possible to do localization and divide the object into small basic geometries where analytical exact and/or approximate solutions can be found. Parallel to the developments in computer memory and speed direct numerical techniques have become feasible.

Analytical solutions are of major interest as test models for comparison with numerical techniques. Gustav Mie solved the problem of electromagnetic scattering from a metallic sphere [1]. The details may also be found in [2]-[3]. A brief review about scattering by imperfectly conducting spheres and the forward- backward scattering results for wide range of radius conductivity and positive / negative permittivity values is given in [4].

Understanding and predicting wave scattering is also important in weather-radar systems. A study in Meteorology dealt with electromagnetic scattering theory and analysis of electromagnetic scattering characteristics of water and ice is presented in [5]. It is assumed that rain drops are spherical so that Mie Solutions can be applied for specified temperatures and related refractive indexes of ice and waters. Also in communication systems, attenuation caused by atmospheric particles at microwave frequency range is obtained by assuming them as spherical and applying Mie Solutions. Related with that, the complex refractive index of raindrops at $20^0 C$ which requires Mie solutions, for different frequencies in microwave region is calculated in [6]. Wiscombe [7] also deals with Mie series and his algorithm is still one of the most powerful and the most accurate one. Also, a new algorithm which uses ratio between Ricatti Bessel functions instead of logarithmic derivative and the comparison between Wiscombe's algorithm is presented in [8].

Method of Moments (MoM) constructs a system of equations in matrix form using electric field integral equation (EFIE). Here, the incident field, location, geometry and electrical parameters (relative permittivity and conductivity of the object) of the object are known. The unknowns are the equivalent volume current densities. The origin and the development of the MoM are fully documented by Harrington [9]. The procedure is essentially same with the weighted residuals method [10]. In this technique, an integral equation (IE) is obtained to satisfy the boundary conditions on the scattering surface in terms of the unknown induced surface current density. Then, the unknown current density is expanded approximately in MoM with different types of basis functions [11]. The basis function is substituted into the original operator of equation and the resulting equation is tested so that the weighted residual is zero.

MoM procedure in finding unknown current distribution may be classified into two groups. The first group deals with the unknown currents where they are distributed over boundary surfaces between linear homogenous and isotropic region. By applying surface equivalence principle [12] electromagnetic field inside the region can be expressed in terms of equivalent electric and magnetic currents distributed on the surface of the object. The procedure categorized as Surface Integral Equation (SIE). Earliest works on 3-D SIE scattering problems [13]-[14] only involve rotationally or axially symmetric perfect electric conductor (PEC) objects. Difficulties in treating MoM for complex structures are because of the representation of the currents near surface junctions and edges which introduce singularities. This deficiency can in principle be overcome by using basis functions containing the correct edge singularity in sub-domains near edges [15]. In 1984, Rao-Wilton-Glisson developed special sub-domain basis functions (RWG) defined over triangular patches for analysis of arbitrary shaped metallic structures [16]. Rao *et al.* extended the method to observe combined metallic and dielectric structures where metallic and dielectric surfaces are infinitesimally close but never touch each other which results relatively large number of unknowns. Thus, it is limited electrically small structures [17].

The determination of unknown currents distributed throughout a linear homogenous and isotropic medium belongs to the second class. They are related with volume integral equations (VIE). For this case, the unknown function is distributed over the volume of material objects. Electric field due to the current carrying volume is expressed in terms of dyadic Green's functions (4.4). When the source and observation points are on the source point, a singularity occurs and the integral in (4.4) becomes improper. Van Bladel excludes the singularity by introducing a principle value integral (PV) [18]. Livesay and Chen developed electric field integral equations (EFIE) by applying PV for 3-D scattering from dielectric bodies [19]. They evaluate the PV integral over a spherical volume is evaluated with lengthy manipulation. Ching-Chang Su evaluated PV integral over a spherical volume was evaluated using symmetry properties of spherical coordinates which represented in much simpler way [20]. In dielectric regions, a piece-wise constant representation of electric field causes errors in the fields for higher relative permittivity values. Hangmann and Levin suggest that accuracy could be obtained by employing smaller cells to discretize the body in the region of the boundaries [21]. Difficulties with original EFIE formulations have motivated the development of techniques for higher order basis functions. Unlike cubic discretization Wilton Shaubert and Glisson extended RWG basis functions of surfaces and suggest tetrahedral cells to discretize VIE [22]. Of course, all suggested works for conventional VIE solutions with MoM require large computer memory for matrix storage involved in computation. To reduce the required storage memory, iterative solutions such as conjugate gradient fast Fourier transform (CG-FFT) method are exploited [23]. Conversely, these kinds of iterative techniques increase computation time. To reduce computational complexity of integral equations, fast algorithms have been studied for several researchers. Nested equivalence principle algorithm that depends on Huygen's equivalence principle [24] is one of them. The algorithm based on dividing the original problem to subgroups until the lowest subgroups are reached The scattering cross section for dielectric cylinder and required computation time are given. In 2000's, Kottman and Martin represented a new algorithm for high permittivity scatterer. To reduce the singularity in source region, the algorithm suggests subtracting a function which has the same singular behavior with the original one from the integrand. [25]. Results show that scattering from dielectric cylinder converges for high size parameters. Recent decades, there are much more efforts to find scattering characters inhomogeneous objects with anisotropic permittivity and permeability tensors [26]. In recent period, Tao and Chen, solve VIE for inhomogenous objects by curvilinear tetrahedral

elements in which the Lagrange interpolation polynomials are utilized to construct the basis functions for representing the unknown volume electric current density.

As previously stated, despite high number unknowns large memory requirement, VIE is more commonly applied procedure for scattering of 3-D penetrable objects. In this study, MoM is applied to VIE to acquire scattering characteristics of arbitrary shaped 3-D objects. RCS calculation of arbitrary 3-D shaped conducting or dielectric objects with different conductivity and relative permittivity values are done. Computations are performed using home-made MATLAB codes. Validation of the numerical approach is done by comparing the scattering results of spheres with analytical Mie solution. RCS definition, characterization in terms of polarization and RCS examination in terms of frequency regions are examined in the following chapter. Next, brief summary is done about Mie theory and MATLAB based Mie codes are given. Discretization of 3-D arbitrary shaped material is examined and matrix equation is given in fourth chapter. Lastly, both monostatic and bistatic scattering examples for spheres with different relative permittivity and conductivity values and the implementation of the MoM algorithm to 3-D canonical examples are shown.

2. RADAR CROSS SECTION (RCS)

2.1 RCS Definition

When an object is exposed to electromagnetic waves, the incident energy of the external wave is scattered in all directions. The spatial distribution of energy depends on several factors such as polarization of the incident wave, physical size and geometry and composition of the object, operating frequency etc. This distribution of energy is called *scattering* the object is called *scatterer*. The intensity of the energy scattered towards the receiver is defined as radar cross section (RCS) of the object. [28] defines RCS as a measure of reflective strength of a target and gives it as 4π times the ratio of the power per unit solid angle scattered in a specified direction to the power per unit area in a plane wave incident on the scatterer from a specified direction.

Solid angle, Ω in steradians (sr) is a two dimensional angle in three dimensional space measuring how large an object appears from a viewing point. Let's define R as a radius of an arbitrary sphere and S' as the spherical surface area then the solid angle is basically equal to the spherical surface area divided by the square of R :

$$\Omega = \iint_{S'} \frac{\vec{n}.d\vec{s}'}{R^2} = \int_0^{2\pi}\int_0^{\pi} \sin\theta' d\theta' d\phi' = 4\pi(\text{sr}) \tag{2.1}$$

Thus, a sphere contains 4π sr. Let the incident power density at scattering target from distance radar be P_i (Watts/m^2), the target captures amount of incident power related with its cross section σP_i (Watts). The captured power can be absorbed or scattered. Assume that the target is isotropic so that it scatters the power uniformly in all 4π sr space. Assume the distance between the radar and the target is R . Therefore, the scattered power density, in Watts/meter^2, is given by

$$P_s = \frac{\sigma P_i}{4\pi R^2} \tag{2.2}$$

(0.1)

Eq. (2.2) can be used to obtain RCS, σ, by considering $R \to \infty$ (in the far field)

$$\sigma = \lim_{R\to\infty} 4\pi R^2 \frac{P_s}{P_i} \tag{2.3}$$

Figure 2.1 depicted the whole scenario. The incident and scattered powers can be expressed in terms of electric (or magnetic) field intensities. Thus, RCS can also be defined as

$$\sigma = \lim_{R\to\infty} 4\pi R^2 \frac{|E_s|^2}{|E_i|^2} \quad \left(OR\ \sigma = \lim_{R\to\infty} 4\pi R^2 \frac{|H_s|^2}{|H_i|^2} \right) , \tag{2.4}$$

where E_s and E_i are the scattered and incident electric field intensities; H_s and H_i are scattered and incident magnetic field intensities at respectively.

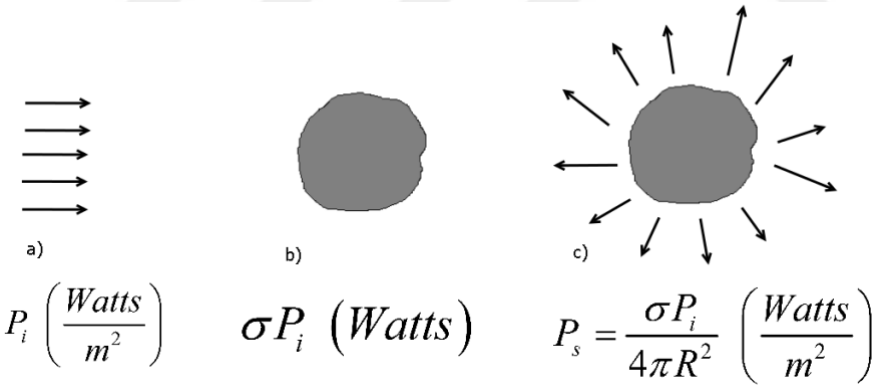

Figure 2.1 Depiction of RCS definition a) incident power flux from distant transmitter b) the scatterer with σ cross section captures σP_i watts of Energy c) the scatterer scatters the captured energy uniformly in all $4\pi\ (sr)$ space.

RCS can also be expressed in logarithmic form:

$$\sigma_{dB} = 10\log_{10}(\sigma). \tag{2.5}$$

For instance, a $\sigma = 0.34m^2$ in dB scale, it corresponds to $10\log_{10}(0.34) = -4.7dB$, or $\sigma_{dB} = 28$ is equal to $10^{28/10} = 631m^2$.

Target RCS is classified in terms of the receiver and transmitter arrangement. In monostatic (backscattering) case, where the angles of incidence and scattering are the same, the receiver and transmitter are collocated; typically same antenna is used as both transmitter and receiver. On the other hand, in bistatic case transmitter and receiver antenna are located in different sites. Thus, angular location of the target depends upon receiver and transmitter.

2.2 Polarization

Electromagnetic waves in RCS prediction are characterized by the direction of incident and scattered fields and their polarization [27]. Polarization specifies the spatial direction of the electric field intensity vector with respect to time. There are three types of polarization; *elliptical circular* and *linear* see, Figure 2.2

Linear Polarization is the simplest type of polarization. At every instant time, if the field intensity vector $\left(\vec{E}(\vec{r}\,) \text{ or } \vec{H}(\vec{r}\,)\right)$ is always pointing in one direction for all points in space, it is linearly polarized. For the linear polarization the field vector has to have only one component or two linearly orthogonal components which have $n\pi\ (rad)$ phase difference ($n \in \mathbf{Z}$)

If the intensity of the field has two orthogonal linear components with same magnitude and $(2n+1)\pi\ (rad)$ phase difference, they trace a circle as a function of time, called *circularly*

polarized. Depending on phase difference; they can be right hand (clockwise) or left hand (counter clockwise) circular polarized.

Elliptical polarization is the most general case of linear and circular cases. To observe an elliptical polarization, the two orthogonal linear components of the field intensity may have different amplitudes. In that case, the phase difference between them must be different from $n\pi\ (rad)$ phase difference. If they have same amplitude, the phase difference cannot be $(2n+1)\pi\ (rad)$. As an example, let the propagation is on z direction, possible plane wave polarizations are depicted in Figure 2.3 (in Figure 2.2 only the electric field intensities are shown).

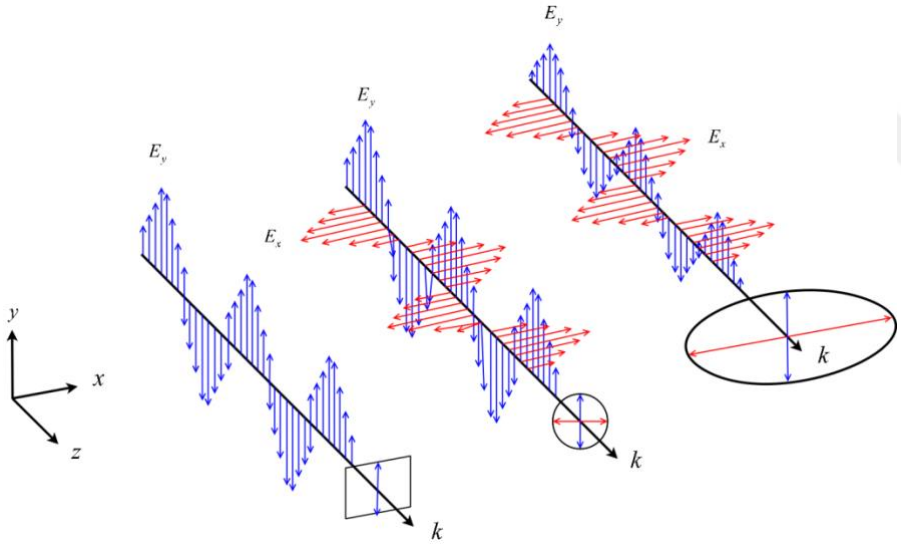

Figure 2.2 Polarization of arbitrary electric field intensities which are plane waves, where the propagation is on z direction. Linearly, circular and elliptic types of polarizations are shown respectively.

An arbitrarily polarized electromagnetic wave may be described in terms of two circularly polarized fields' summation [29]. Lets define an electric field intensity which is the summation of right hand (RCP) and left hand (LCP) circularly polarized field intensities:

$$\vec{E}(\vec{r}) = \vec{E}(\vec{r})_{RCP} + \vec{E}(\vec{r})_{RCP}. \tag{2.6}$$

Similarly, $\vec{E}_{RCP}$ and $\vec{E}_{LCP}$ are fields can be described as

$$\begin{aligned}\vec{E}(\vec{r})_{RCP} &= \vec{E}(\vec{r})_V + i\vec{E}(\vec{r})_H \\ \vec{E}(\vec{r})_{LCP} &= \vec{E}(\vec{r})_V - i\vec{E}(\vec{r})_H .\end{aligned} \tag{2.7}$$

In (2.7), $\vec{E}(\vec{r})_V$ and $\vec{E}(\vec{r})_H$ are represent vertical and horizontal polarizations, respectively. RCS is a far field quantity; therefore spherical coordinate system is convenient to describe incident and scattered fields [27]. Vertical and horizontal polarizations can be described in terms of θ and φ angles of spherical coordinate system, respectively. For example an incident -or scattered- electric field may be either $\vec{E}(\vec{r})_\theta$ or $\vec{E}(\vec{r})_\varphi$,called theta (vertical) or phi-polarized (horizontal) waves. Figure 2.3 depicts a sample scenario. An arbitrary target is located at the origin, where both the incidence from which the incident wave –not the propagation vector- comes, and scatter angles are indicated by θ, the vertical angle from z axis and φ, the angle from horizontal axis in the xy plane. The angle of propagation vector determines the direction of RCS. For backscatter RCS computations incident and scattered angles are equal.

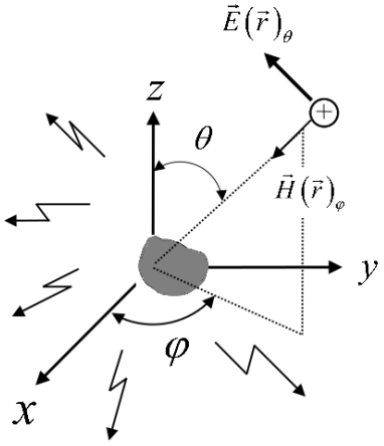

Figure 2.3 An arbitrary target located at the origin, illuminated by a theta-polarized EM wave. The two angles θ and φ are vertical and horizontal angles respectively are shown. The theta-polarized EM wave has components $\vec{E}(\vec{r})_\theta$ and $\vec{H}(\vec{r})_\varphi$

Basically, RCS of a target depends upon the transmitter and receiver; therefore, the polarization is classified into two class called co-polarized and cross polarized owing to the incident and scattered fields. Table 2.1 shows the four possible cases.

Table 2.1 Co- and Cross Polarized RCS cases

Incident Field	**Scattered Field**	**RCS Polarization Type**

Vertical (θ)	Vertical (θ)	Co-polarized $(\sigma_{VV}$ OR $\sigma_{\theta\theta})$
Vertical (θ)	Horizontal (φ)	Cross polarized $(\sigma_{VH}$ OR $\sigma_{\theta\varphi})$
Horizontal (φ)	Horizontal (φ)	Co-polarized $(\sigma_{HH}$ OR $\sigma_{\varphi\varphi})$
Horizontal (φ)	Vertical (θ)	Cross polarized $(\sigma_{HV}$ OR $\sigma_{\varphi\theta})$

As mentioned above, RCS as a scalar number, is a function of the polarization of the incident and scattered wave. Polarization scattering matrix gives complete description about the relationship between the incident and scattered waves. Let the incident electric field vector be $\vec{E}_i$ and the scattered field be $\vec{E}_s$. In matrix notation the relationship between them is shown with scattering matrix $\bar{S}$

$$\vec{E}_s = \bar{S}\vec{E}_i , \tag{2.8}$$

and can be generalized in terms of theta and phi components

$$\begin{bmatrix} \vec{E}_{s\theta} \\ \vec{E}_{s\varphi} \end{bmatrix} = \begin{bmatrix} S_{\theta\theta} & S_{\theta\varphi} \\ S_{\varphi\theta} & S_{\varphi\varphi} \end{bmatrix} \begin{bmatrix} \vec{E}_{i\theta} \\ \vec{E}_{i\varphi} \end{bmatrix}$$
$$S_{\theta\theta} = \sqrt{\sigma_{\theta\theta}} \tan^{-1}\left(\frac{\mathrm{Im}\left\{ \vec{E}_{s\varphi} / \vec{E}_{i\theta} \right\}}{\mathrm{Re}\left\{ \vec{E}_{s\varphi} / \vec{E}_{i\theta} \right\}} \right) \tag{2.9}$$

2.3 Frequency Domain

In addition to the polarization of incident and scattered fields, frequency of incident wave and the geometry of the target are also crucial concept to determine RCS. Let the target has dimension l and the wavelengths of incident wave is lambda (λ). Depending upon l and λ, three distinctive RCS frequency regions are [29]:

- *Rayleigh Region*
- *Resonance (Mie) Region*
- *Optical Region.*

Low frequency region is also known as Rayleigh region where the target dimension is much less than the radar wavelength $(l << \lambda)$. In this region, the situation is equivalent to static field problem except that incident field is changing in time. Amplitude and phase variation over body length is little. RCS is proportional to the fourth power of frequency $(\sigma \propto f^4)$ and to the square of the volume of the target [27]

The region where the target dimension and the wavelength are of the same order $(l \approx \lambda)$ is called the Resonance (Mie) region. The geometry and material of a target completely contributes to its RCS and therefore analytical methods are rarely applicable. In addition to analytical ones, frequency and time domain numerical methods like Method of Moments and Finite Difference Time Domain can be applied in this regime. Mie theory which describes the analytical solution of scattering on a sphere is explained in next chapter in detail.

In high frequency region (optical region), dimension of the target is much larger than the wavelength $(l >> \lambda)$. RCS is roughly the same size as the real area of the target. High frequency approximations such as Geometrical Optics (GO), Physical Optics (PO), the Geometrical Theory of Diffraction (GTD) Physical Theory of Diffraction (PTD) and the Uniform Theory of Diffraction (UTD) are applied to investigate dominant parts of the targets like reflecting planes edges etc. The illustration of RCS over these three regions is that of a perfect electric conducting (PEC) sphere with a radius a, is shown in Figure 2.4, where RCS has been normalized to the projected area of the sphere, πa^2, plotted as a function of sphere circumference normalized to wavelength, $k_0 a = 2\pi a / \lambda_0$.

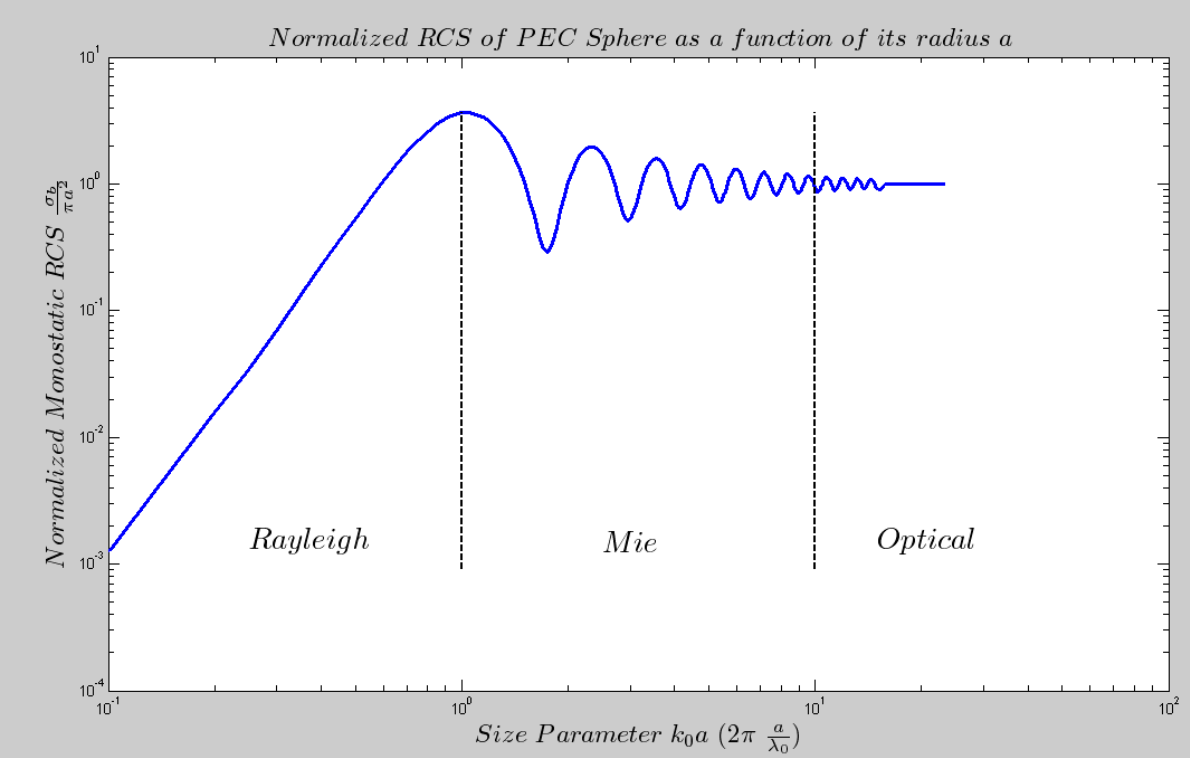

Figure 2.4 Normalized mono-static RCS of PEC Sphere as a function of its radius, showing the three regimes: Rayleigh, Mie and Optical.

3. MIE THEORY

In 1908, Gustav Mie solved the problem of electromagnetic scattering from a metallic sphere [1]. This solution is now usually called the Mie theory [2] It is also possible to extend the solution to any arbitrary homogenous dielectric sphere. The solution to the problem depends on the expansion of incident plane wave in a series of spherical vector harmonics. The scattered and absorbed fields are acquired due to appropriate boundary conditions. Here, a summary of Mie theory is given (see [2], for details).

3.1 Scalar Wave Equation

A scalar function $f(r,\theta,\varphi)$ which satisfies scalar Helmholtz equation in spherical coordinates is given by

$$\frac{1}{r^2}\frac{\partial}{\partial r}\left(r^2\frac{\partial f}{\partial r}\right)+\frac{1}{r^2\sin\theta}\frac{\partial}{\partial\theta}\left(\sin\theta\frac{\partial f}{\partial\theta}\right)+\frac{1}{r^2\sin\theta}\frac{\partial^2 f}{\partial\varphi^2}+k^2 f=0. \tag{3.1}$$

Assume (3.1) is separable [34] writing $f(r,\theta,\varphi)=f_r(R)\,f_\theta(\theta)\,f_\varphi(\varphi)$ yields three one dimensional equations:

$$\frac{d^2 f_\varphi}{d\varphi^2}+m^2 f_\varphi=0, \tag{3.2}$$

$$\frac{1}{\sin\theta}\frac{d}{d\theta}\left(\sin\theta\frac{df_\theta}{d\theta}\right)+\left(p^2-\frac{m^2}{\sin^2\theta}\right)=0, \tag{3.3}$$

$$r^2\frac{d^2 f_R}{dr^2}+2r\frac{df_r}{dr}+\left(k^2r^2-p^2\right)f_r=0. \tag{3.4}$$

Here, p and m are separation constants. Physically, it is required that at any arbitrary fixed point in space the field must be single valued. Thus, $f(r,\theta,\varphi)$ is a single valued function in azimuth angle. Under these conditions, the separation constant m must be either zero or positive integer. Therefore linearly independent solutions of (3.2) are:

$$\begin{aligned} f_{\varphi(even)} &= \cos m\varphi \\ f_{\varphi(odd)} &= \sin m\varphi. \end{aligned} \tag{3.5}$$

To determine the constant p, it is needed to look at associated Ordinary Legendre differential equation. For any arbitrary variable α, the function of $\alpha\left(g(\alpha)\right)$ is a Legendre polynomial if it satisfies Ordinary Legendre differential equation, which is given as:

$$\left(1-\alpha^2\right)\frac{d^2g(\alpha)}{d\alpha}+2\alpha\frac{dg(\alpha)}{d\alpha}+n(n+1)g(\alpha)=0. \tag{3.6}$$

When (3.3) is compared with (3.6), it is observed that f_θ is an associated Legendre function with $\alpha=\cos\theta$, due to that, (3.3) may be re-written in terms of $\alpha=\cos\theta$:

$$\left(1-\alpha^2\right)\frac{d^2f_\theta}{d\alpha}+2\alpha\frac{df_\theta}{d\alpha}+\left[p^2-\frac{m^2}{1-\alpha^2}\right]f_\theta=0. \tag{3.7}$$

For $p^2=n(n+1)$ with $n=0,1,2,3...$, there is an ascending convergent series at poles $\alpha=\pm1$ (a few first terms break off then converges), called Legendre Polynomials $P_n(\alpha)$. If it is differentiated m times with respect to α (3.7) becomes

$$f_\theta(\theta)=P_n^m(\cos\theta)=\left(1-\cos^2\theta\right)^{m/2}\frac{d^mP_n(\cos\theta)}{(d\cos\theta)^m} \tag{3.8}$$

Lastly, the solution of radial part $f_R(R)$ may be found using normalization $f_R(R)=\sqrt{kR}v(R)$. In this case, $v(R)$ satisfies (3.4)

$$r^2\frac{d^2v}{dr^2}+2r\frac{dv}{dr}+\left[k^2r^2-\left(n+\frac{1}{2}\right)^2\right]v=0 \tag{3.9}$$

Two linearly independent solutions of (3.3) are Bessel functions of the first and second kinds:

$$j_\nu(kr)=\frac{1}{\sqrt{kr}}J_{n+1/2}(kr) \tag{3.10}$$

$$y_\nu(kr)=\frac{1}{\sqrt{kr}}Y_{n+1/2}(kr). \tag{3.11}$$

There are modified Bessel functions which are called Spherical Bessel functions. They have all the features like recurrence of Bessel and Hankel functions [30]. The linearly independent combinations of (3.10) and (3.11) lead to Spherical Hankel functions.

$$h_\nu^{(1)}(kr)=j_\nu(kr)+iy_\nu(kr) \tag{3.12}$$

$$h_\nu^{(2)}(kr)=j_\nu(kr)-iy_\nu(kr). \tag{3.13}$$

The asymptotic behaviors of these functions are [30]:

$$\lim_{x\to\infty}j_\nu(x)\to\frac{1}{x}\cos\left(x-\frac{\nu+1}{2}\pi\right) \tag{3.14}$$

$$\lim_{x\to\infty}y_\nu(x)\to\frac{1}{x}\sin\left(x-\frac{\nu+1}{2}\pi\right) \tag{3.15}$$

Asymptotic behaviors of spherical Hankel functions are:

$$\lim_{x\to\infty}h_\nu^{(1)}(x)\to\frac{(-i)^\nu e^{ix}}{ix}, \tag{3.16}$$

$$\lim_{x\to\infty} h_\nu^{(2)}(x) \to -\frac{(i)^\nu e^{-ix}}{ix}. \tag{3.17}$$

Also, around zero, second order spherical Bessel function goes to infinity

$$\lim_{x\to 0} y_\nu(x) \to \infty. \tag{3.18}$$

The radial part of the solution can be any of (3.10) (3.11) (3.12) and (3.13). However, physically, the wave created by a finite source, which should be outgoing; not incoming wave. Thus, due to (3.18) second order spherical Bessel function cannot be a solution of the radial part. Selected solutions can be $h_\nu^{(1)}$ and $h_\nu^{(2)}$. They are conjugate pairs. Selecting one of them depends upon the time convention. In this study, $e^{-i\omega t}$ is assumed, therefore, $h_\nu^{(1)}$ represent the incoming wave According to (3.14), the behavior of spherical Bessel function at far away is a kind of cosine function which leads us a standing wave.

To sum up, the scalar function $f(r,\theta,\varphi)$ has two independent solutions which can be also defined as even and odd parts:

$$f_{emn} = \cos(m\varphi) P_n^m(\cos\theta) z_n(kr) \tag{3.19}$$

$$f_{mn(even)} = \sin(m\varphi) P_n^m(\cos\theta) z_n(kr), \tag{3.20}$$

where, $z_n(kr)$ is spherical Bessel or Hankel function of the first kind with order n. The choice about which is the solution depends on the position of the wave.

3.2 Vector Wave Equations and Spherical Harmonics

Helmholtz has stated that it is possible to determine a vector uniquely if its divergence of curl is known [2]. Three vectors related with scalar functions given in (3.19) and (3.20) will be defined. Their divergence and curl are determined so that they becomes single valued due to Helmholtz's theory. Next, it is shown that these vectors are appropriate to represent electric and magnetic field intensities.

Let's define an arbitrary constant vector $\vec{c}$ it is possible to construct three vectors as follows:

$$\begin{aligned} \vec{L} &= \nabla f \\ \vec{M} &= \nabla \times (\vec{c} f) \\ \vec{N} &= \frac{1}{k} \nabla \times \vec{M}. \end{aligned} \tag{3.21}$$

Since $\vec{c}$ is a constant vector, it is obvious that $\vec{M}$ can be written as:

$$\vec{M} = \vec{L} \times \vec{c} = \frac{1}{k} \nabla \times \vec{N}. \tag{3.22}$$

Due to (3.22) $\vec{M}$ is perpendicular to $\vec{L}$ $\left(\vec{L} \cdot \vec{M} = 0\right)$. Thus, curl and divergence of $\vec{L}$ due to (3.21) and (3.22) are:

$$\begin{aligned} \nabla \times \vec{L} &= 0 \\ \nabla \cdot \vec{L} &= \nabla^2 f = -k^2 f. \end{aligned} \tag{3.23}$$

Furthermore, related with (3.21) and (3.22) $\vec{M}$ and $\vec{N}$ are solenoidal; their divergence is zero

$$\nabla \cdot \vec{M} = \nabla \cdot \vec{N} = 0. \tag{3.24}$$

Thus, vectors $\vec{L}, \vec{M}, \vec{\mathrm{N}}$ are single valued, continuous in a given domain and form a discrete set. An arbitrary wave function can be represented as a linear combination of these vector functions. In addition, in free space plane wave solution of field intensities, are divergences free and for each is proportional to the curl of the other. Thus, $\vec{M}$ and $\vec{\mathrm{N}}$ vectors are appropriate to represent the field intensities $\vec{E}(\vec{r})$ and $\vec{H}(\vec{r})$. If $\vec{c}$ is selected as $\vec{e}_r$, radial unit vector of sphere, than, $\vec{M}$

will be tangent to any sphere. $\vec{M}$ and $\vec{\mathrm{N}}$ vectors are called vector harmonics. The scalar function $f(r,\theta,\varphi)$ is usually called generating functions [2], [3], [30].

Related with (3.19), (3.20) and (3.21) $\vec{M}$ and $\vec{\mathrm{N}}$ vectors have also even and odd parts which are shown as:

$$\vec{M}_{emn} = \nabla \times \left(\vec{e}_r f_{emn}\right) \tag{3.25}$$

$$\vec{M}_{omn} = \nabla \times \left(\vec{e}_r f_{omn}\right) \tag{3.26}$$

$$\vec{N}_{emn} = \frac{1}{k} \nabla \times \vec{M}_{emn} \tag{3.27}$$

$$\vec{N}_{emn} = \frac{1}{k} \nabla \times \vec{M}_{emn}, \tag{3.28}$$

Where f_{emn} and f_{omn} are mutually orthogonal functions and form a complete orthogonal set [34]. An arbitrary function which satisfies Helmholtz equation in spherical coordinates can be represented as infinite series in terms of f_{emn} and f_{omn}. They are in the form of spherical harmonics.

Next step is writing the fields (incident scattered and refracted) in terms of $\vec{M}$ & $\vec{N}$ vectors in series summation. From (3.25) - (3.28), it is possible to write:

$$\vec{M}_{emn} = -\vec{e}_\theta \frac{m}{\sin\varphi} \sin m\varphi P_n^m(\cos\theta) z_n(kr) - \vec{e}_\varphi \cos m\varphi \frac{dP_n^m(\cos\theta)}{d\theta} z_n(kr) \tag{3.29}$$

$$\vec{M}_{omn} = \vec{e}_\theta \frac{m}{\sin\varphi} \sin m\varphi P_n^m(\cos\theta) z_n(kr) - \vec{e}_\varphi \sin m\varphi \frac{dP_n^m(\cos\theta)}{d\theta} z_n(kr) \tag{3.30}$$

$$\vec{N}_{emn} = \vec{e}_R \frac{z_n(kr)}{(kr)} \cos m\varphi n(n+1) P_n^m(\cos\theta)$$
$$+\vec{e}_\theta \cos m\varphi \frac{dP_n^m(\cos\theta)}{d\theta} \frac{1}{kr} \frac{d}{d(kr)}\left(krz_n(kr)\right) \tag{3.31}$$
$$-\vec{e}_\varphi m \sin m\varphi \frac{P_n^m(\cos\theta)}{\sin\theta} \frac{d}{d(kr)}\left(krz_n(kr)\right)$$

$$\vec{N}_{omn} = \vec{e}_R \frac{z_n(kr)}{(kr)} \sin m\varphi n(n+1) P_n^m(\cos\theta)$$
$$+\vec{e}_\theta \sin m\varphi \frac{dP_n^m(\cos\theta)}{d\theta} \frac{1}{kr} \frac{d}{d(kr)}\left(krz_n(kr)\right) \tag{3.32}$$
$$+\vec{e}_\varphi m \cos m\varphi \frac{P_n^m(\cos\theta)}{\sin\theta} \frac{d}{d(kr)}\left(kRz_n(kr)\right).$$

3.3 Expansion of the Plane Wave in Vector Harmonics

Suppose we have a plane wave propagating along z direction and polarized in the x direction:

$$\vec{E}_i(\vec{r}) = \vec{e}_x E_0 e^{ikz}$$
$$\left(\vec{e}_x = \vec{e}_r \cos\varphi \sin\theta + \vec{e}_\theta \cos\varphi \cos\theta + \vec{e}_\varphi \sin\varphi\right). \tag{3.33}$$

The radial component of this wave can be written as

$$\vec{E}_i = \cos\varphi \sin\theta \vec{E}_i = E_0 \frac{\cos\varphi}{jkr} \frac{\partial}{\partial\theta}\left(e^{ikr\cos\theta}\right). \tag{3.34}$$

Incident field can be written in terms of spherical harmonics:

$$\vec{E}_i = \sum_{m=0}^{\infty}\sum_{n=0}^{\infty}\left[B_{emn}\vec{M}_{emn} + B_{omn}\vec{M}_{omn} + A_{emn}\vec{N}_{emn} + A_{omn}\vec{N}_{omn} \right], \tag{3.35}$$

and the coefficients can be found from:

$$B_{emn} = \frac{\int_0^{2\pi}\int_0^{\pi} \vec{E}_i.\vec{M}_{emn} \sin\theta d\theta d\varphi}{\int_0^{2\pi}\int_0^{\pi} \left|\vec{M}_{emn}\right|^2 \sin\theta d\theta d\varphi} \quad B_{omn} = \frac{\int_0^{2\pi}\int_0^{\pi} \vec{E}_i.\vec{M}_{omn} \sin\theta d\theta d\varphi}{\int_0^{2\pi}\int_0^{\pi} \left|\vec{M}_{omn}\right|^2 \sin\theta d\theta d\varphi} \ . \tag{3.36}$$

$$A_{emn} = \frac{\int_0^{2\pi}\int_0^{\pi} \vec{E}_i.\vec{N}_{emn} \sin\theta d\theta d\varphi}{\int_0^{2\pi}\int_0^{\pi} \left|\vec{N}_{emn}\right|^2 \sin\theta d\theta d\varphi} \quad \mathrm{A}_{omn} = \frac{\int_0^{2\pi}\int_0^{\pi} \vec{E}_i.\vec{N}_{omn} \sin\theta d\theta d\varphi}{\int_0^{2\pi}\int_0^{\pi} \left|\vec{N}_{omn}\right|^2 \sin\theta d\theta d\varphi} \ . \tag{3.37}$$

Due to orthogonal properties of sine and cosine functions for all m and n and the remaining coefficients are also zero except $m=1$. Superscript (1) will be used to emphasize that radial dependence of incident field is $j_n(kr)$. Thus, the incident electric field intensity becomes:

$$\vec{E}_i = \sum_{n=0}^{\infty}\left(B_{o1n}\vec{M}_{o1n}^{(1)} + A_{e1n}\vec{N}_{e1n}^{(1)} \right). \tag{3.38}$$

The coefficients are derived from the orthogonality relations:

$$\begin{aligned} &\int_0^{2\pi}\int_0^{\pi} \vec{e}_x \cdot\vec{M}_{o1n}^{(1)} e^{ikR\cos\theta} \sin\theta d\theta d\varphi = 2\pi i^n n(n+1)\left(j_n(kr) \right)^2, \\ &\int_0^{2\pi}\int_0^{\pi} \vec{e}_x \cdot\vec{N}_{e1n}^{(1)} e^{ikR\cos\theta} \sin\theta d\theta d\varphi = -2\pi i^{n+1} n(n+1)\left[n(n+1)\left(j_{n+1}(kr) \right)^2 \right]. \end{aligned} \tag{3.39}$$

The denominator integral of (3.36) and (3.37) for $m=1$ are calculated as

$$\int_0^{2\pi}\int_0^{\pi}\left|\vec{M}_{o1n}^{(1)}\right|^2\sin\theta d\theta d\varphi=\frac{2\pi}{2n+1}\frac{(n+1)!}{(n-1)!}n(n+1)\left[j_n(kr)\right]^2,$$
$$\int_0^{2\pi}\int_0^{\pi}\left|\vec{N}_{e1n}^{(1)}\right|^2\sin\theta d\theta d\varphi=\frac{2\pi}{(2n+1)}\frac{(n+1)!}{(n-1)!}n(n+1)\left[n(n+1)\left(j_{n+1}(kr)\right)^2\right]. \tag{3.40}$$

with $\vec{B}_{o1n}$ and $\vec{A}_{e1n}$ equal to

$$\vec{B}_{o1n}=E_0\frac{2n+1}{n(n+1)}i^n,$$
$$\vec{A}_{e1n}=E_0\frac{2n+1}{n(n+1)}i^{n+1}. \tag{3.41}$$

The incident field defined in (3.38) becomes

$$\vec{E}_i=E_0\sum_{n=0}^{\infty}i^n\frac{2n+1}{n(n+1)}\left(\vec{M}_{o1n}^{(1)}-i\vec{N}_{e1n}^{(1)}\right). \tag{3.42}$$

The magnetic field intensity, the curl of the incident electric field intensity, is represented as:

$$\vec{H}_i=\frac{-k}{\omega\mu}E_0\sum_{n=0}^{\infty}i^n\frac{2n+1}{n(n+1)}\left(\vec{M}_{o1n}^{(1)}-i\vec{N}_{e1n}^{(1)}\right). \tag{3.43}$$

At boundaries, tangential parts of the incident $\left(\vec{E}_i,\vec{H}_i\right)$ scattered $\left(\vec{E}_s,\vec{H}_s\right)$ and the transmitted $\left(\vec{E}_t,\vec{H}_t\right)$ fields must be continuous. Orthogonality of the vector harmonics and continuity of boundary conditions forced scattered and transmitted fields in the form of expansion of spherical harmonics also. Related with the asymptotic behavior, given in (3.14)-(3.18), physically, as the transmitted field must be finite at the origin, radial part of the transmitted field must be in the form of Spherical Bessel function $j_n(k_1R)$. (k_1 is the wave number inside sphere)

$$\vec{E}_t = \sum_{n=0}^{\infty}\left(c_n\vec{M}_{o1n}^{(1)} - id_n\vec{N}_{e1n}^{(1)}\right),$$
$$\vec{H}_t = \frac{-k}{\omega\mu}\sum_{n=0}^{\infty}\left(d_n\vec{M}_{e1n}^{(1)} - ic_n\vec{N}_{o1n}^{(1)}\right). \tag{3.44}$$

The scattered field is an outgoing wave, and for $e^{-i\omega t}$ time-dependence asymptotic behavior of the Hankel function, and determined time convention the radial part of the scattered field must be in the form of $h_n^{(1)}\left(k_0 R\right)$ (k_0 is the wave number of out of space, which is free space generally):

$$\vec{E}_s = \sum_{n=0}^{\infty}\left(ia_n\vec{N}_{e1n}^{(3)} - b_n\vec{M}_{o1n}^{(3)}\right),$$
$$\vec{H}_s = \frac{k}{\omega\mu}\sum_{n=0}^{\infty}\left(ib_n\vec{N}_{o1n}^{(3)} + a_n\vec{M}_{e1n}^{(3)}\right). \tag{3.45}$$

Hence, all the fields are in the series form of spherical harmonics weighted by some constants.

The constants a_n, b_n, c_n, d_n are determined from the boundary conditions

3.4 Boundary conditions and the constants

Suppose the sphere has a radius a $\left(r = a\right)$. The tangential fields are continuous:

$$\left(\vec{E}_i + \vec{E}_s - \vec{E}_t\right)\times\vec{e}_r = \left(\vec{H}_i + \vec{H}_s - \vec{H}_t\right)\times\vec{e}_r = 0. \tag{3.46}$$

Expanding (3.46) four independent solutions for four unknowns are acquired:

$$
\begin{aligned}
E_{\theta i} + E_{\theta s} &= E_{\theta t} \\
E_{\varphi i} + E_{\varphi s} &= E_{\varphi t} \\
H_{\theta i} + H_{\theta s} &= H_{\theta t} \\
H_{\varphi i} + H_{\varphi s} &= H_{\varphi t}.
\end{aligned}
\tag{3.47}
$$

Solving (3.47) yields

$$
a_n = \frac{j_n(Na)\left[(k_0a)\, j_n(k_0a)\right]' - j_n(k_0a)\left[(Nk_0a)\, j_n(Nk_0a)\right]'}{j_n(Nk_0a)\left[(k_0a)\, h_n^{(1)}(k_0a)\right]' - h_n^{(1)}(k_0a)\left[(Nk_0a)\, j_n(Nk_0a)\right]'}
\tag{3.48}
$$

$$
b_n = \frac{j_n(a)\left[(Nk_0a)\, j_n(Nk_0a)\right]' - N^2 j_n(Nk_0a)\left[(k_0a)\, j_n(k_0a)\right]'}{h_n^{(1)}(k_0a)\left[(Nk_0a)\, j_n(Nk_0a)\right]' - N^2 j_n(Nk_0a)\left[(k_0a)\, h_n^{(1)}(k_0a)\right]'}
\tag{3.49}
$$

$$
c_n = \frac{i/(k_0a)}{h_n^{(1)}(k_0a)\left[(Nk_0a)\, j_n(Nk_0a)\right]' - j_n(Nk_0a)\left[(k_0a)\, h_n^{(1)}(k_0a)\right]'}
\tag{3.50}
$$

$$
d_n = \frac{i/(k_0a)}{h_n^{(1)}(k_0a)\left[(Nk_0a)\, j_n(Nk_0a)\right]' - N^2 j_n(Nk_0a)\left[(k_0a)\, h_n^{(1)}(k_0a)\right]'}
\tag{3.51}
$$

where again $k_0 = \omega\sqrt{\mu_0\varepsilon_0}$ is the wave number of free space; and $k_1 = k_0\sqrt{\varepsilon}$ is the wave number of the sphere. Note that k_1 may be complex depending on conductivity of the medium, and $N = \frac{k_1}{k_0}$ is the refractive index of the sphere. Owing to (3.44) and (3.45) it is possible to say that a_n & b_n are scattering coefficients; whereas c_n & d_n are the coefficients of the transmitted field inside the medium (sphere). By introducing Ricatti Bessel functions

$$
\begin{aligned}
\psi_n(r) &= r j_n(r), \\
\xi_n(r) &= r h_n^{(1)}(r).
\end{aligned}
\tag{3.52}
$$

Thus, the scattering coefficients become:

$$a_n = \frac{N\psi_n(Nk_0a)\psi_n'(k_0a) - \psi_n(k_0a)\psi_n'(Nk_0a)}{N\psi_n(Nk_0a)\xi_n'(k_0a) - \xi_n(k_0a)\psi_n'(Nk_0a)},$$
$$b_n = \frac{\psi_n(Nk_0a)\psi_n'(k_0a) - N\psi_n(k_0a)\psi_n'(Nk_0a)}{\psi_n(Nk_0a)\xi_n'(k_0a) - N\xi_n(k_0a)\psi_n'(Nk_0a)}. \quad (3.53)$$

Depending on the conductivity of the sphere, the arguments of the Ricatti Bessel function $\psi(Nk_0a)$ are generally complex; so that the function and its derivative diverge after few terms for lossy mediums. Especially for PEC spheres, numerical calculations are limited. However, logarithmic derivative of $D_n(Nk_0a)$ of $\psi_n(Nk_0a)$ [3], [7]:

$$D_n(Nk_0a) = \frac{\psi'(Nk_0a)}{\psi(Nk_0a)} = \frac{\left[(Nk_0a)\, j_n(Nk_0a)\right]'}{(Nk_0a)\, j_n(Nk_0a)}, \quad (3.54)$$

is remains finite except for $k_0a \to 0$. Let's define a complex argument $s = Nk_0a$, $D_n(s)$ satisfies the downward recurrence (lower order terms are generated from higher order terms) relations

$$D_{n-1}(s) = \frac{n}{s} - \frac{1}{D_n(s) + n/s}. \quad (3.55)$$

The scattering coefficients, given in (3.53) can be written in terms of (3.54) and (3.55) as

$$a_n = \frac{\left(\frac{D_n(Nk_0a)}{N} + \frac{n}{k_0a}\right)\psi_n(k_0a) - \psi_{n-1}(k_0a)}{\left(\frac{D_n(Nk_0a)}{N} + \frac{n}{k_0a}\right)\xi_n(k_0a) - \xi_{n-1}(k_0a)}$$
$$b_n = \frac{\left(ND_n(Nk_0a) + \frac{n}{k_0a}\right)\psi_n(k_0a) - \psi_{n-1}(k_0a)}{\left(ND_n(Nk_0a) + \frac{n}{k_0a}\right)\xi_n(k_0a) - \xi_{n-1}(k_0a)}. \quad (3.56)$$

The calculation of the coefficients required n terms where $n \to \infty$. However, according to [17] it is sufficient to accept iteration number as $n \approx 2 + k_0 a + 16 k_0 a^{1/3}$.

A short MATLAB code is developed to calculate the scattering coefficients. This code is given in Table 3.1. The code needs refractive index N and the size parameter $k_0 a$ as input and give the coefficients a_n and b_n as output

Table 3.1: A MATLAB script to calculate scattering coefficients a_n and b_n

```
%=========================================================================
%   Program  : ab_Mie(N,kr).m
%   Author   : Ahmet SEFER
%   Date     : Nov 2013
%   Purpose  : To Compute a matrix of Mie coefficients, a_n, b_n,
%                 of orders from n=1 to nmax
%      N      : complex refractive index; N=N'+iN"
%      kr     : k0*a size parameter; k0 is wave number in free space, a is
%                 radius of sphere
%=========================================================================

%%
function results=ab_Mie(N,kr)


nmax=round(2+kr+4.*kr.^(1/3));     %Iteration number

Nkr=N.*kr;                    %refractive index times size parameter

nmx=round(max(nmax,abs(Nkr))+16);

n=(1:nmax); nu = (n+0.5);

spherical_const=sqrt(0.5*pi*kr);   %constant for spherical bessel functions

%%
%==========RICATTI BESSEL FUNCTIONS According to (3.52) ==================

%nth term of Ricatti Bessel "psi" function
Ricatti_Psi_n =spherical_const.*besselj((nu),kr);
```

```
%(n-1)th term of Ricatti Bessel "psi" function
Ricatti_Psi_n_1=ones(1,nmax);
Ricatti_Psi_n_1(2:nmax)=spherical_const.*besselj(nu(1:end-1),kr);
Ricatti_Psi_n_1(1) =sin(kr);


%nth term of Ricatti Bessel "chi" function
Ricatti_Chi_n =-spherical_const.*bessely((nu),kr);

%(n-1)th term of Ricatti Bessel "psi" function
Ricatti_Chi_n_1    =ones(1,nmax);
Ricatti_Chi_n_1(2:nmax)=-spherical_const.*bessely(nu(1:end-1),kr);
Ricatti_Chi_n_1(1) =cos(kr);

%nth term of Ricatti Bessel "xi" function
Ricatti_xi_n=Ricatti_Psi_n-1i*Ricatti_Chi_n;

%(n-1)th term of Ricatti Bessel "xi" function
Ricatti_xi_n_1=Ricatti_Psi_n_1-1i*Ricatti_Chi_n_1;

%=========================================================================

%%
%================ Computation of Dn(z) According to (3.55)=================
dn(nmx)=0+0i;

for j=nmx:-1:2

   dn(j-1)=j./Nkr-1/(dn(j)+j./Nkr);

end;

Dn=dn(n);          % Dn(z), n=1 to nmax

da=Dn./N+n./kr;

db=N.*Dn+n./kr;
%=========================================================================

%%
%==========  SCATTERING COEFFICINETS According to (3.56)  ================%

an=(da.*Ricatti_Psi_n-Ricatti_Psi_n_1)./(da.*Ricatti_xi_n-Ricatti_xi_n_1);

bn=(db.*Ricatti_Psi_n-Ricatti_Psi_n_1)./(db.*Ricatti_xi_n-Ricatti_xi_n_1);
```

```
results=[an;bn];
end
%=========================================================================

%%
```

3.5 Extinction Absorption Forward and Radar Cross-sections of Sphere

As explained in the previous section, a plane wave, impinged on an object causes several distinct effects. The particle may convert some of the energy contained in the beam into other forms of energy, such as heat. This phenomenon is called *absorption*. Second, it extracts some of the incident energy and scatters it in all directions at the frequency of the incident wave. This phenomenon is called *scattering.* As a result of absorption and scattering the energy of the incident beam is reduced by an amount equal to the sum of the absorbed and scattered energy. This reduction is called *extinction*. [35]

Due to asymptotic behaviors of spherical Hankel and Bessel functions given in (3.14) - (3.18) the scattered fields, given in (3.45), in the far field region can be defined as:

$$E_{s\theta} = \eta H_{s\varphi} \cong i\frac{e^{ik_1 r}}{k_1 r}\cos\varphi S_2(\theta)$$
$$E_{s\varphi} = \eta H_{s\theta} \cong i\frac{e^{ik_1 r}}{k_1 r}\sin\varphi S_1(\theta), \tag{3.57}$$

where $S_1(\theta)$ and $S_2(\theta)$ are amplitude functions:

$$S_1(\theta)=\sum_{n=1}^{\infty}\frac{2n+1}{n(n+1)}\left[a_n\pi_n(\cos\theta)+b_n\tau_n(\cos\theta)\right],$$
$$S_2(\theta)=\sum_{n=1}^{\infty}\frac{2n+1}{n(n+1)}\left[a_n\tau_n(\cos\theta)+b_n\pi_n(\cos\theta)\right]. \quad (3.58)$$

$\pi_n(\cos\theta)=\frac{P_n^1(\cos\theta)}{\sin\theta}$ & $\tau_n(\cos\theta)=\frac{dP_n^1(\cos\theta)}{d\theta}$ are nothing new; may be named as angle dependent functions [3].The MATLAB code which calculates the angle dependent functions and amplitude functions are given in Table 3.2 and Table 3.3, respectively.

Table 3.2 A MATLAB script to calculate angle dependent functions π_n and τ_n

```
function result=Mie_pitau(N,kr,u)

%=================================================================
=
%   Program : Mie_pitau(u,lmax).m
%   Author  : Ahmet SEFER
%   Date    : Nov 2013
%   Purpose : To Compute angular dependent functions pi_n and tau_n from 1
%                 to nmax
%     u       : Specified theta angle in radians
%=================================================================
=

%%
ab=ab_Mie(N,kr);
nmax=length(ab(1,:));

% first and second values of the functions pi_n and tau_n
p(1)=1;
t(1)=cos(u);
p(2)=3*cos(u);
t(2)=3*cos(2*u);
%%
%recurrance relations of the functions
for ii=3:nmax,
p1=(2*ii-1)./(ii-1).*p(ii-1).*cos(u);
p2=ii./(ii-1).*p(ii-2);
p(ii)=p1-p2;
```

```
t1=ii*cos(u).*p(ii);
t2=(ii+1).*p(ii-1);
t(ii)=t1-t2;
end;
%%
result=[p;t];
```

Table 3.3 A MATLAB script to calculate amplitude functions

```
function result = Mie_S12(N,kr,u)

%=======================================================================
%   Program : Mie_S12(N,kr,u).m
%   Author   : Ahmet SEFER
%   Date      : Nov 2013
%   Purpose : To Compute Mie Scattering functions S1 and S2
%      N        : complex refractive index; N=N'+iN''
%      kr       : k0*a size parameter; k0 is wave number in free space, a is
%                  radius of sphere
%      u        :Specified theta angle in radians
%=======================================================================
=

%%
ab  =ab_Mie(N,kr);          %Scattering Coefficients
an  =ab(1,:);
bn  =ab(2,:);
nmax=length(ab(1,:));       %Iteration number
pt  =Mie_pitau(N,kr,u);     %Angle Dependent Functions given in (3.58)
pin =pt(1,:);               %Pn1/sin(theta) Pn1= Legendre
taun=pt(2,:);               %d/dt(pin)

n=(1:nmax);
n2=(2*n+1)./(n.*(n+1));     %The coefficient shown in (3.58)
pin=n2.*pin;
taun=n2.*taun;

%================Amplitude Functions According to (3.58)==================%
S1=(an*pin'+bn*taun');
```

```
S2=(an*taun'+bn*pin');

result=[S1;S2];
```

Sphere scattered energy can be defined using the (3.57) and (3.58) as:

$$\begin{aligned} W_s &= \frac{1}{2}\operatorname{Re}\int_0^{2\pi}\int_0^{\pi}\left(E_\theta H_\varphi^* - E_\varphi H_\theta^*\right)R^2\sin\theta d\theta d\varphi \\ &= \frac{\pi|E_0|^2}{2k_1^2\eta}\operatorname{Re}\int_0^{\pi}\left(\left|S_1(\theta)\right|^2 + \left|S_2(\theta)\right|^2\right)\sin\theta d\theta. \end{aligned} \tag{3.59}$$

The energy density of the incident plane wave defined in (3.42) is

$$P = \frac{|E_0|^2}{2\eta} = \frac{1}{2}|E_0|^2\sqrt{\frac{\varepsilon}{\mu}}. \tag{3.60}$$

The RCS (σ_{scat}), may then be defined as [10]

$$\sigma_{scat} = \frac{W_s}{P}. \tag{3.61}$$

From (3.58) absolute square of amplitude functions are defined as

$$\begin{aligned} \left|S_1(\theta)\right|^2 &= \sum_{n=1}^{\infty}\sum_{m=1}^{\infty}\frac{(2n+1)(2m+1)}{n(n+1)m(m+1)}\left[a_n a_m^*\tau_n\tau_m + b_n b_m^*\pi_n\pi_m + a_n b_m^*\tau_n\pi_m + a_m^* b_n\tau_m\pi_n\right], \\ \left|S_2(\theta)\right|^2 &= \sum_{n=1}^{\infty}\sum_{m=1}^{\infty}\frac{(2n+1)(2m+1)}{n(n+1)m(m+1)}\left[a_n a_m^*\pi_n\pi_m + b_n b_m^*\tau_n\tau_m + a_n b_m^*\pi_n\tau_m + a_m^* b_n\pi_m\tau_n\right]. \end{aligned} \tag{3.62}$$

Note that, angle dependent functions are orthogonal Legendre type functions [30]:

$$\int_0^{\pi}\left(\pi_n\pi_m+\tau_n\tau_m\right)=\delta_{nm}\frac{2\left[n\left(n+1\right)m\left(m+1\right)\right]}{2n+1},$$

where, δ_{nm} is Kronecker-delta function: $\delta_{nm}=\begin{Bmatrix}1 & if\ n=m\\ 0 & elsewhere\end{Bmatrix}$

Finally, the normalized RCS is given as:

$$\frac{\sigma_s}{\pi a^2}=\frac{2}{\left(k_0a\right)^2}\sum_{n=1}^{\infty}\left(2n+1\right)\left(\left|a_n\right|^2+\left|b_n\right|^2\right). \tag{3.63}$$

The forward scattering theorem states that the total cross-section σ_{ext} is related to the real part of the scattering amplitude in the forward direction (direction of incident wave) $\theta=0$ [36]. Note that $\pi_n\left(\cos\theta\right)\big|_{\theta=0}=\tau_n\left(\cos\theta\right)\big|_{\theta=0}=\frac{n\left(n+1\right)}{2}$ and therefore extinction cross section normalized to geometrical cross section of the sphere with radius a becomes

$$\begin{aligned}&\frac{\sigma_{ext}}{\pi a^2}=\frac{2}{\left(k_1a\right)^2}\mathrm{Re}\left\{S_1\left(0\right)\right\}=\frac{2}{\left(k_1a\right)^2}\mathrm{Re}\left\{S_2\left(0\right)\right\},\\ &OR\\ &\frac{\sigma_{ext}}{\pi a^2}=\frac{2}{\left(k_1a\right)^2}\sum_{n=1}^{\infty}\left(2n+1\right)\mathrm{Re}\left\{a_n+b_n\right\}.\end{aligned} \tag{3.64}$$

The absorption cross section is the difference of extinction and scattered cross section [36]:

$$\sigma_a=\sigma_{ext}-\sigma_s. \tag{3.65}$$

(RCS) of the sphere is defined as

$$\sigma_b = \lim_{R\to\infty} 4\pi R^2 \left.\frac{|E_s|^2}{|E_i|^2}\right|_{\theta=\pi} . \tag{3.66}$$

Since,

$$\pi_n(\cos\theta)\big|_{\theta=\pi} = -\tau_n(\cos\theta)\big|_{\theta=\pi} = -(-1)^n \frac{n(n+1)}{2} ;$$

RCS of the sphere with radius a normalized to geometrical cross section is defined as RCS efficiency, and equals to

$$Q_b = \frac{\sigma_b}{\pi a^2} = \frac{2}{(k_0 a)^2}\left|\sum_{n=1}^{\infty}(-1)^n(2n+1)(a_n - b_n)\right|^2 . \tag{3.67}$$

As an example, take the RCS of water droplet at wavelength $\lambda_0 = 3.2$ cm with a complex refractive index $N_{water} = 7.1 - 2.89i$ at $0^0 C$ [5]. Ice, on the other hand, has a complex refractive index $N_{ice} = 1.78 - 2.4\times10^{-3} i$ [18] for the same wavelength. Their normalized radar cross sections as a function of normalized circumference $k_0 a = 2\pi \frac{a}{\lambda_0}$ are shown in Figure 3.1.

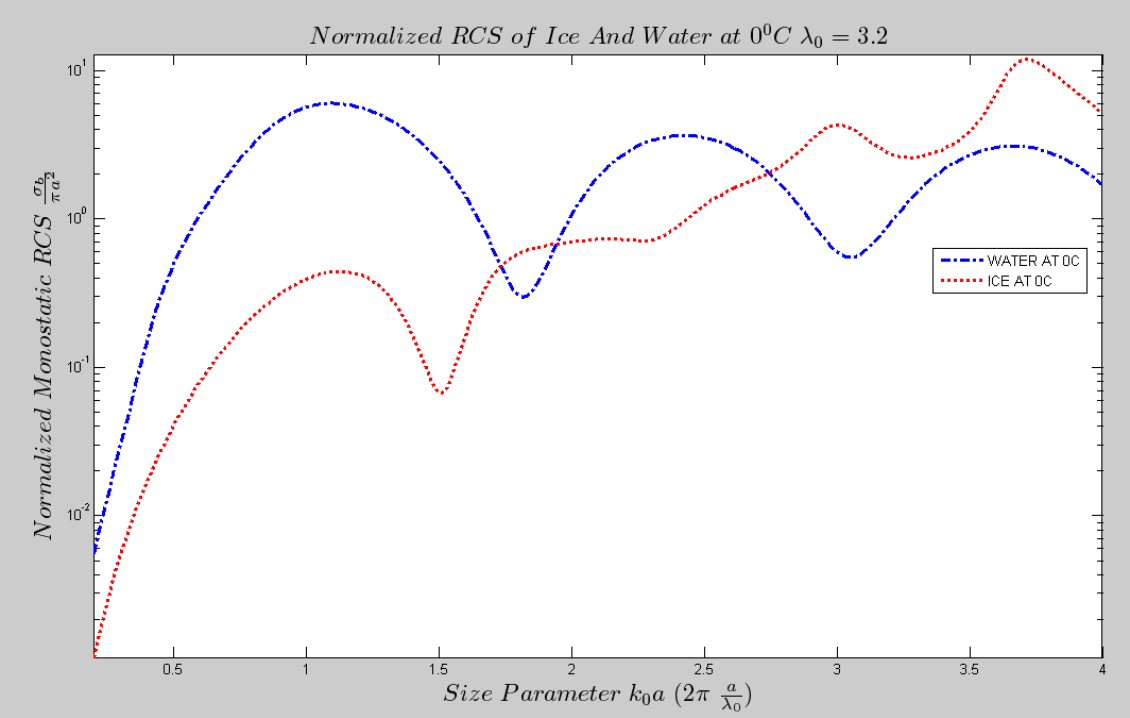

Figure 3.1 Normalized RCS of water and ice droplets at 0^0C

4. SCATTERING OF ARBITRARY THREE DIMENSIONAL OBJECTS IN FREE SPACE MEDIUM

4.1 Statement of the Problem

Mie Theory, explained in the previous section, addresses a 3-D analytical solution of scattering problem for a spherical medium in resonance region. However, to acquire more general results, such as obtaining RCS not only spherical but also of arbitrary shaped structures, there are powerful frequency and time domain numerical methods. Method of Moments (MoM), detailed in [12], is one of powerful frequency domain numerical methods. It uses a discrete mesh model of a target. Through the method, electric field integral equations (EFIE) -or magnetic field integral equations (MFIE) - is solved via reducing them to a matrix problem with a matrix size directly related to the electrical size of the target.

To begin with, guiding the scattering problem, it is handled an arbitrary shaped non magnetic object with its volume V constitutive parameters conductivity $\sigma(\vec{r})$, dielectric permittivity $\varepsilon(\vec{r})$ and free space magnetic permeability $\mu(\vec{r}) = \mu_0$, is embedded in the free space with permittivity ε_0 and permeability μ_0. The object is illuminated by an incident plane wave as shown in Figure 4.1. Knowing the incident field and the constitutive parameters of the object, the total electric field strength can be solved via volume integral equation (VIE) [18-26], namely;

$$\vec{E}_i(\vec{r}) = \vec{E}(\vec{r}) - i\omega\mu_0 \int_{\vec{r}' \in V} \bar{\bar{G}}(\vec{r}, \vec{r}')\, \vec{J}(\vec{r}')\, dV. \tag{4.1}$$

Here, the term $\bar{\bar{G}}(\vec{r}, \vec{r}')$ is free space dyadic Green's function and is explained in detail in section 4.2. The current density $\vec{J}(\vec{r})$ can be expressed in terms of electric field and the medium parameters due to the volume equivalence theorem [11] as in (4.2)

$$\vec{J}(\vec{r}) = \left[\sigma(\vec{r}) - i\omega\left(\varepsilon(\vec{r}) - \varepsilon_0\right)\right]\vec{E}(\vec{r}). \tag{4.2}$$

Let the wave number inside the medium be $\vec{k}(\vec{r}) = \omega\sqrt{\mu_0\varepsilon_0\varepsilon_r}\sqrt{1+\frac{\sigma(\vec{r})}{i\omega\varepsilon_0}}$, which is a function of position, and the wave number of outside be the free space wave number $k_0 = \omega\sqrt{\mu_0\varepsilon_0}$. Related to (4.2) and the defined wave numbers, an "object function" can be defined as:

$$v(\vec{r}) = \frac{k(\vec{r})}{k_0} - 1. \tag{4.3}$$

The object function $v(\vec{r})$ is also called "the electrical constant function". Note that, outside the medium $k(\vec{r}) = k_0$ and the object function given in (4.3) is equals to zero. Due to (4.2) and (4.3), one can show that VIE, given in (4.1), becomes Fredholm integral Equation of second kind where the unknown total electric field strength is inside and outside the integral is:

$$\vec{E}_i(\vec{r}) = \vec{E}(\vec{r}) - k_0^2 \int_{\vec{r}' \in V} \bar{\bar{G}}(\vec{r},\vec{r}')v(\vec{r}')E(\vec{r})dV. \tag{4.4}$$

The total electric field, $\vec{E}(\vec{r})$ at an arbitrary point inside the object in free space is the sum of the incident field $\vec{E}_i(\vec{r})$ and the scattered field $\vec{E}_s(\vec{r})$, generated by the volume current density inside the object, given in (4.2), $\vec{J}(\vec{r})$, namely;

$$\vec{E}(\vec{r}) = \vec{E}_i(\vec{r}) + \vec{E}_s(\vec{r}). \tag{4.5}$$

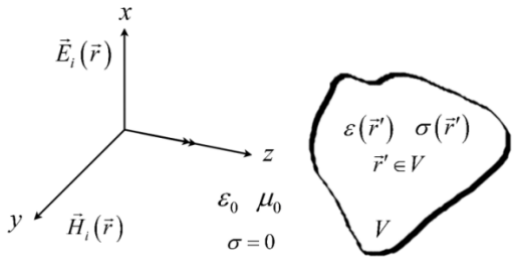

Figure 4.1 An arbitrary object illuminated by a plane electromagnetic wave is located in free space. As an example, direction of propagation is on $\vec{e}_z$ and the directions of the fields are normal to each other and propagation

Taking into consideration (4.4) and (4.5), one can easily obtain the expression for the scattered field for the problem shown in Figure 4.1

$$\vec{E}_s(\vec{r}) = k_0^2 \int_{\vec{r}' \in V} \bar{\bar{G}}(\vec{r},\vec{r}')v(\vec{r}')E(\vec{r}')dV. \tag{4.6}$$

In (4.6), $\vec{r} = (x, y, z)$ and $\vec{r}' = (x', y', z')$ stand for observation and source locations respectively. If the source point and observation point placed on the same location, $\bar{\bar{G}}(\vec{r},\vec{r}')$ contains a singularity of the order of $|\vec{r} - \vec{r}'|^{-3}$ The integral defined in (4.6) becomes improper. To be able to overcome this, an infinitesimal volume surrounding the sub-domain $\vec{r} = \vec{r}'$ is excluded and this process is called Principle Value (PV) [18]. According to this, (4.6) becomes

$$\vec{E}_i(\vec{r}) = k_0^2 PV \left\{ \int_V \bar{\bar{G}}(\vec{r},\vec{r}')v(\vec{r}')E(\vec{r}')dV \right\} - v(\vec{r}')E(\vec{r}')\bar{\bar{L}} \tag{4.7a}$$

$$\vec{E}_i(\vec{r}) = k_0^2 \lim_{V_\delta \to 0} \int_{V - V_\delta} \bar{\bar{G}}(\vec{r},\vec{r}')v(\vec{r}')E(\vec{r}')dV - v(\vec{r}')E(\vec{r}')\bar{\bar{L}}. \tag{4.7b}$$

In (4.7a) and (4.7b), $\bar{\bar{L}}$ is a correction term, called "source dyadic" and depends solely shape of the removed volume. Physically, because the exclusion volume will cause discontinuous currents on the surface of the volume, surface charges will accumulate on the surface, which will cause an electrostatic field inside the volume. This electromagnetic field will persist no matter how small the volume is, and is a function of the geometry of the volume. In this study spherical volume is considered as excluded volume and represented by Van Bladel [18] as

$$\bar{\bar{L}} = \frac{\bar{\bar{I}}}{3}, \tag{4.8}$$

where $\bar{\bar{I}}$ is the unit dyadic.

4.2 Dyadic Green's Function & Matrix Transformation

As a generalized definition, Green's function is the impulse response of the system. From electromagnetic point of view, scalar Green's function is simply the impulse response to the scalar Helmholtz Equation by applying appropriate boundary conditions [11]. Differ from scalar case, when the source of the system is handled as vector, a much more complicated Green's functions which are in the form called *dyadic* (see [31], for details). There are several methods to attain dyadic Green's function, the classical approach; attaining the dyadic functions from scalar Green's functions [32] is considered in this work.

Mathematically, scalar Green's Function satisfies the wave equation in free space

$$\nabla^2 g(\vec{r},\vec{r}') + k_0^2 g(\vec{r},\vec{r}') = -\delta(\vec{r}-\vec{r}') \tag{4.9}$$

a solution may explicitly be given as

$$g(\vec{r},\vec{r}') = \frac{e^{ik_0|\vec{r}-\vec{r}'|}}{4\pi|\vec{r}-\vec{r}'|}. \tag{4.10}$$

And the dyadic Green's function can be given in closed form as:

$$\bar{\bar{G}}(\vec{r},\vec{r}') = \left(\bar{\bar{I}} + \frac{1}{k_0^2}\nabla\nabla\right) g(\vec{r},\vec{r}'). \tag{4.11}$$

In (x,y,z) Cartesian coordinates, (4.11) becomes

$$\begin{aligned} &x_1 = x \qquad x_2 = y \qquad x_3 = z; \\ &\bar{\bar{G}}_{x_p x_q}(\vec{r},\vec{r}') = \left(\delta_{pq} + \frac{1}{k_0^2}\frac{\partial^2}{\partial x_p \partial x_q}\right) g(\vec{r},\vec{r}'), \\ &p,q = 1,2,3. \end{aligned} \tag{4.12}$$

$$\delta_{pq} = \begin{cases} 1 & if\ p = q \\ 0 & elsewhere \end{cases}. \tag{4.13}$$

$\bar{\bar{G}}(\vec{r},\vec{r}') = \left[G_{x_p x_q} \right]$ in (4.12) is a 3×3 symmetrical matrix .

4.3 Discretization of the Problem and MoM Procedure

It is possible to transform (4.7b) into matrix equations by MoM. The process begins with discretizing the volume of the object located in free space into N cubical sub-volumes which may be denoted by v_m $(m = 1,2,3...N)$. The spherical volume which has been discretized by cubic sub-volumes is depicted in Figure 4.2. Conveniently to the MoM procedure, the sub-volumes should be as small as to accept that fields $\vec{E}(\vec{r})$ and the object function $v(\vec{r})$ are constant in each sub-volume. Suppose that m^{th} sub-volume is denoted as V_m and its interior point denoted by r_m . For each r_m one re-considers the equation (4.7b) as

$$E_{x_p}(\vec{r}) = E_{i_{x_p}}(\vec{r}) + PV\left\{ \int_V k_0^2 v(\vec{r}') \left[\sum_{q=1}^{3} G_{x_p x_q}(\vec{r},\vec{r}') E_{x_q}(\vec{r}) \right] dv' \right\}, \tag{4.14a}$$

$$E_{x_p}(\vec{r}_m) = E_{i_{x_p}}(\vec{r}_m) + \sum_{q=1}^{3}\sum_{n=1}^{N} k_0^2 v(\vec{r}_n) PV\left[\int_{V_n} G_{x_p x_q}(\vec{r}_m,\vec{r}') dv' \right] E_{x_q}(\vec{r}_n). \tag{4.14b}$$

In (4.14a) and (4.14b) Let the PV integral be defined as:

$$PV\left[\int_{V_n} G_{x_p x_q}(\vec{r}_m,\vec{r}') dv \right] = G^{mn}_{x_p x_q}(\vec{r}_m,\vec{r}'). \tag{4.15}$$

Due to (4.15), the whole discretized system becomes

$$E_{x_p}(\vec{r}_m) - \sum_{q=1}^{3}\sum_{n=1}^{N} k_0^2 v(\vec{r}_n) G^{mn}_{x_p x_q}(\vec{r}_m,\vec{r}') E_{x_q}(\vec{r}_n) = E^{i}{}_{x_p}(\vec{r}_m). \tag{4.16}$$

The total and incident electric field intensities due to the segmented body become N dimensional vectors and $G^{mn}_{x_p x_q}(\vec{r}_m, \vec{r}')$ become an element of $N \times N$ matrix:

$$\left[E_{x_p}\right] = \begin{bmatrix} E_{x_p}(r_1) \\ E_{x_p}(r_2) \\ \cdot \\ \cdot \\ \cdot \\ E_{x_p}(r_N) \end{bmatrix} \quad \& \quad \left[E_{i_{x_p}}\right] = \begin{bmatrix} E_{i_{x_p}}(r_1) \\ E_{i_{x_p}}(r_2) \\ \cdot \\ \cdot \\ \cdot \\ E_{i_{x_p}}(r_N) \end{bmatrix} \quad ,(p = 1,2,3). \tag{4.17}$$

$$G_{x_p x_q} = \begin{bmatrix} G^{11}_{x_p x_q}(\vec{r}_1, \vec{r}') & G^{12}_{x_p x_q}(\vec{r}_1, \vec{r}') & \cdots & G^{1n}_{x_p x_q}(\vec{r}_1, \vec{r}') & \cdots & G^{1N}_{x_p x_q}(\vec{r}_1, \vec{r}') \\ G^{21}_{x_p x_q}(\vec{r}_2, \vec{r}') & G^{N2}_{x_p x_q}(\vec{r}_2, \vec{r}') & \cdots & G^{2n}_{x_p x_q}(\vec{r}_2, \vec{r}') & \cdots & G^{2N}_{x_p x_q}(\vec{r}_2, \vec{r}') \\ \vdots & & & & & \\ G^{m1}_{x_p x_q}(\vec{r}_m, \vec{r}') & G^{m2}_{x_p x_q}(\vec{r}_m, \vec{r}') & \cdots & G^{mn}_{x_p x_q}(\vec{r}_m, \vec{r}') & \cdots & G^{mN}_{x_p x_q}(\vec{r}_m, \vec{r}') \\ \vdots & & & & & \\ G^{N1}_{x_p x_q}(\vec{r}_N, \vec{r}') & G^{N2}_{x_p x_q}(\vec{r}_N, \vec{r}') & \cdots & G^{Nn}_{x_p x_q}(\vec{r}_N, \vec{r}') & \cdots & G^{NN}_{x_p x_q}(\vec{r}_N, \vec{r}') \end{bmatrix}. \tag{4.18}$$

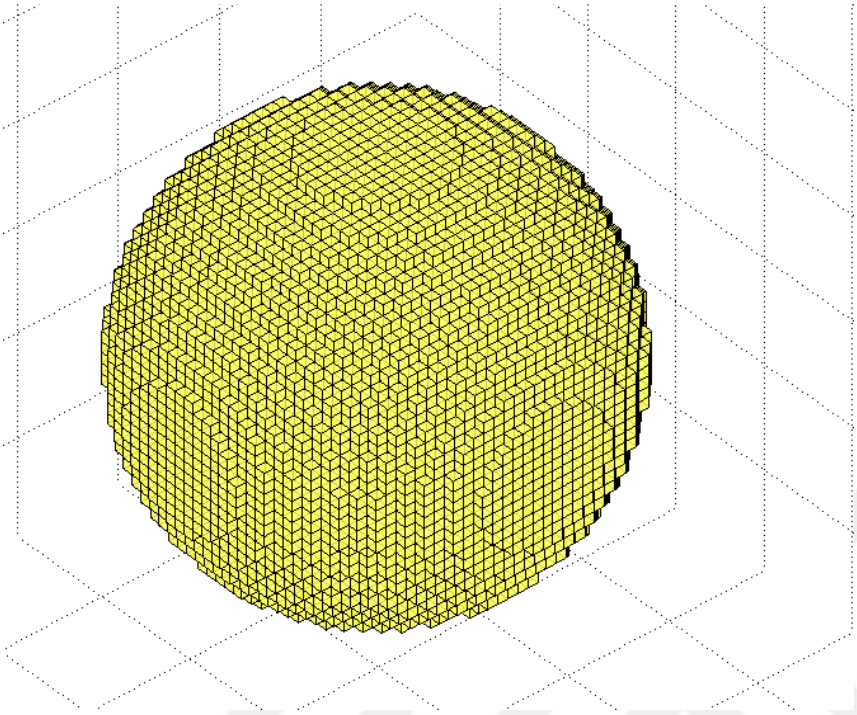

Figure 4.2 The Spherical body is discretized by small cubic volumes denoted as V_n

Assume that a_{eq} is the radius of the small sphere. Matrix elements are examined into two parts: Singular and Non-singular. Obviously, there is no singularity for non-diagonal elements but needs to be calculated PV integral of the diagonal elements for singularities. For non-singular parts of the sub-matrix (non-diagonal) elements of (4.18) are

$$\begin{aligned} &(m \neq n) \\ &G_{pq}^{mn} = D_3 \left[\delta_{pq} + \frac{1}{k_0^2} \frac{\partial^2}{\partial_{x_p} \partial_{x_q}} \right] g(\vec{r}, \vec{r}'); \\ &D_3 = \frac{4\pi a_{eq}}{k_0^2} \left[\frac{\sin(k_0 a_{eq})}{k_0 a_{eq}} - \cos(k_0 a_{eq}) \right]. \end{aligned} \tag{4.19}$$

Here, D_3 is called geometric factor [33] and can be obtained by expanding Scalar Green's function in terms of spherical harmonics, the readers interested in derivation of geometric factor

referred to [33]. On the other hand, for the singular case, when the source and observation are on the same cell G_{pq}^{mm} may be calculated as

$$G_{pq}^{mm} = \delta_{pq} \left\{ \frac{1}{3k_0^2} \left[2\left(1 - ik_0 a_{eq}\right) e^{ik_0 a_{eq}} - 3 \right] \right\}. \tag{4.20}$$

The calculation of $G_{x_p x_q}^{mn}\left(\vec{r}, \vec{r}_m'\right)$ for singular case is given in *Appendix A* in detail.

5. COMPARISON OF NUMERICAL & ANALYTICAL RESULTS

Code validation of the 3D MoM algorithm and data verification is done in two subsections. Section 5.1 belongs to scattering from a PEC sphere where analytical reference solution is available. Here, numerical results obtained using the 3D MoM model is compared with the numerical data obtained using analytical Mie Series formulae. Both isotropic dielectric and conducting spheres are used in the comparisons. For the sake of simplicity, for all spherical cases, the radius of the sphere is selected as $4\ cm$. Far field locations are selected $20\ m$ away from the sphere. In Section 5.2, a few other canonical geometries are used for the validation and verification tests. Examples include a PEC plate, a PEC dihedral, and a PEC trihedral and their RCS behaviors are simulated for different illumination angles. The 3D MoM model is tested against a commercial software package, *CST Microwave Studio®,* which use the FDTD model.

5.1 Analytical & Numerical Results for Sphere

The first example is a loss-free dielectric sphere with zero conductivity. The dielectric constant is $\varepsilon_r = 2$. Monostatic case is assumed. Analytic results are based on Mie series expansion. Numerical results belong to 3D MoM algorithm. Minimum and maximum frequencies are selected as $0.2GHz$ and $1.8GHz$. The first results are shown in Figure 5.1. The solid line and dots belong to Mie series summation nd 3D MoM algorithm, respectively.

The second example in Figure 5.2 belongs to a lossy dielectric with the conductivity σ = 0.02 S/m and relative dielectric constant ε_r = 3.5. The simulations are performed for the same frequency range.

As observed in the figure, the agreement between analytical and numerical results starts to disagree as the frequency increases. In this example, the sphere is discretized by $\lambda_0 / 60$ where λ_0 is the wavelength of free space in the specified frequency. This discrepancy can be removed by

selecting higher discretization ratio. On the other hand, this increases the size of the MoM matrix system which means more memory and longer computation times.

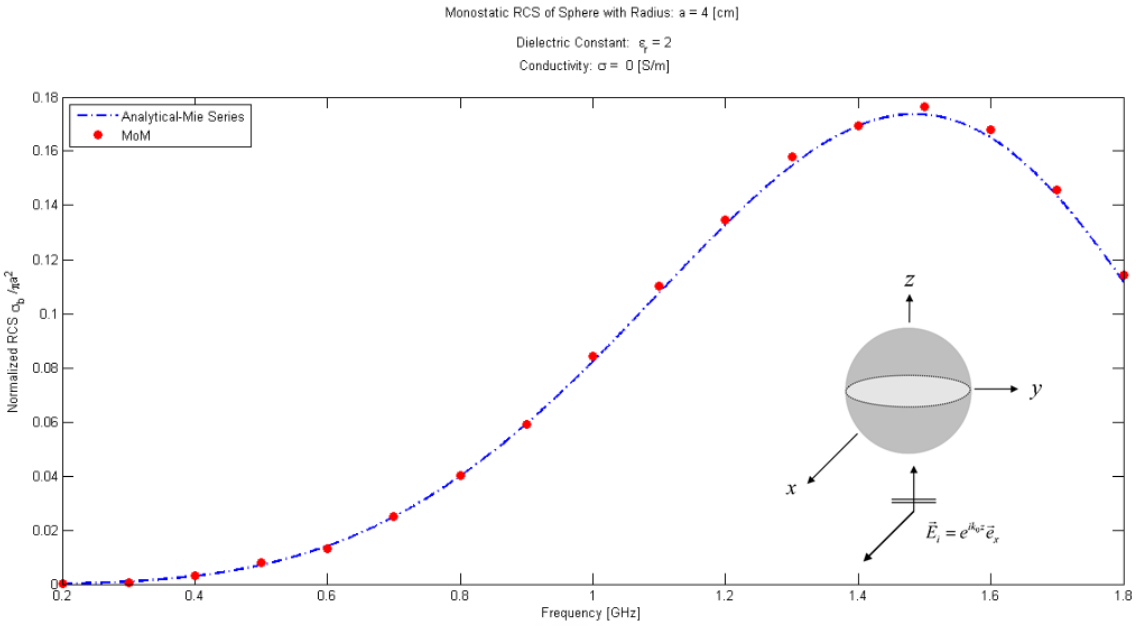

Figure 5.1 Analytical and Numerical monostatic RCS of a dielectric sphere with radius $4\ cm$. $\varepsilon_r = 2$ and σ = 0 S/m. The illumination of the incident wave is also pictured ($\theta_i = 0^0$ $\varphi_i = 0^0$, $\theta_s = 180^0$ $\varphi_s = 0^0$)

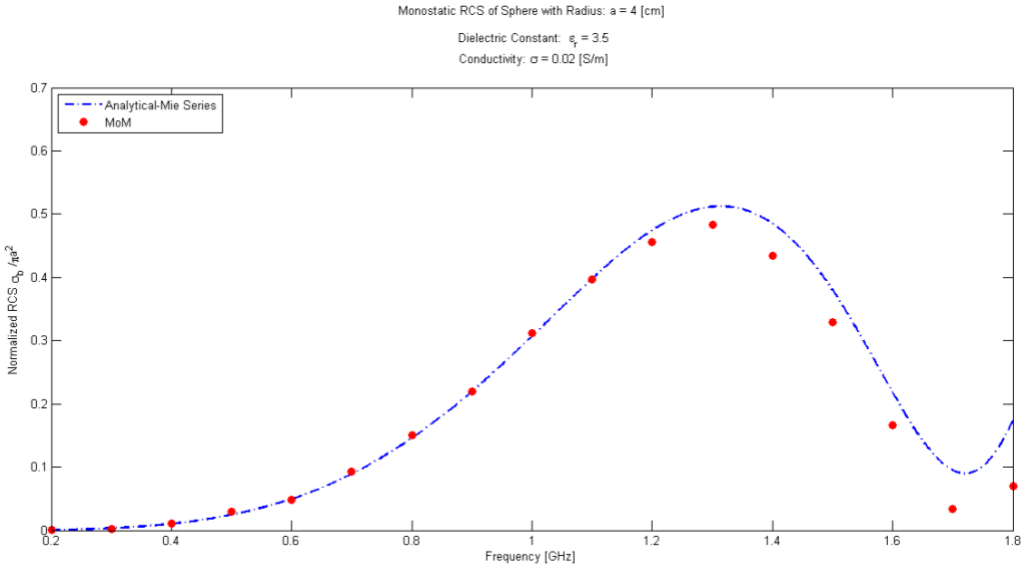

Figure 5.2 Analytical and numerical monostatic RCS of a dielectric sphere with radius $4\ cm$: $\varepsilon_r = 3.5$ and σ = 0.02 S/m. ($\theta_i = 0^0\ \ \varphi_i = 0^0,\ \theta_s = 180^0\ \ \varphi_s = 0^0$)

The third example in Figure 5.3 shows the result for the same relative dielectric constant ($\varepsilon_r = 3.5$) but a smaller conductivity values σ = 0.01 S/m. The same discretization number is used and results are much better than the previous example.

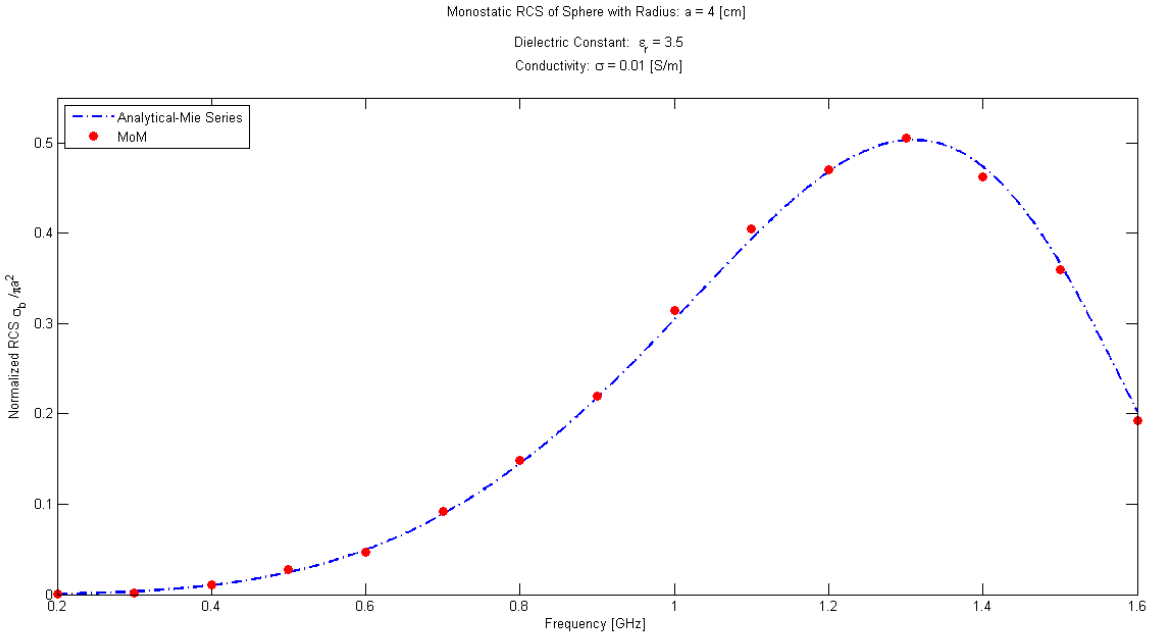

Figure 5.3 Analytical and Numerical monostatic RCS of dielectric sphere with radius $4\ cm$: $\varepsilon_r = 3.5$ and σ = 0.01 S/m ($\theta_i = 0^0\ \ \varphi_i = 0^0,\ \theta_s = 180^0\ \ \varphi_s = 0^0$)

The next example in Figure 5.4 shows the results for the sphere with $\varepsilon_r = 5$ and σ = 0.03 S/m. Here, the sphere is discretized by $\lambda_0 / 150$ instead of $\lambda_0 / 60$. Due to the memory of the computer the simulations are performed up to $1.4GHz$. Better numerical results are obtained for higher discretization of the sphere.

The last example of monostatic case is for a higher dielectric constant. Results given in Figure 5.5 for the sphere with $\varepsilon_r = 7$ and σ = 0.02 S/m with the discretization of $\lambda_0 / 100$ instead of

$\lambda_0 / 150$ to be able to attain more data in Mie region. The simulations are performed up to $1.5GHz$

.

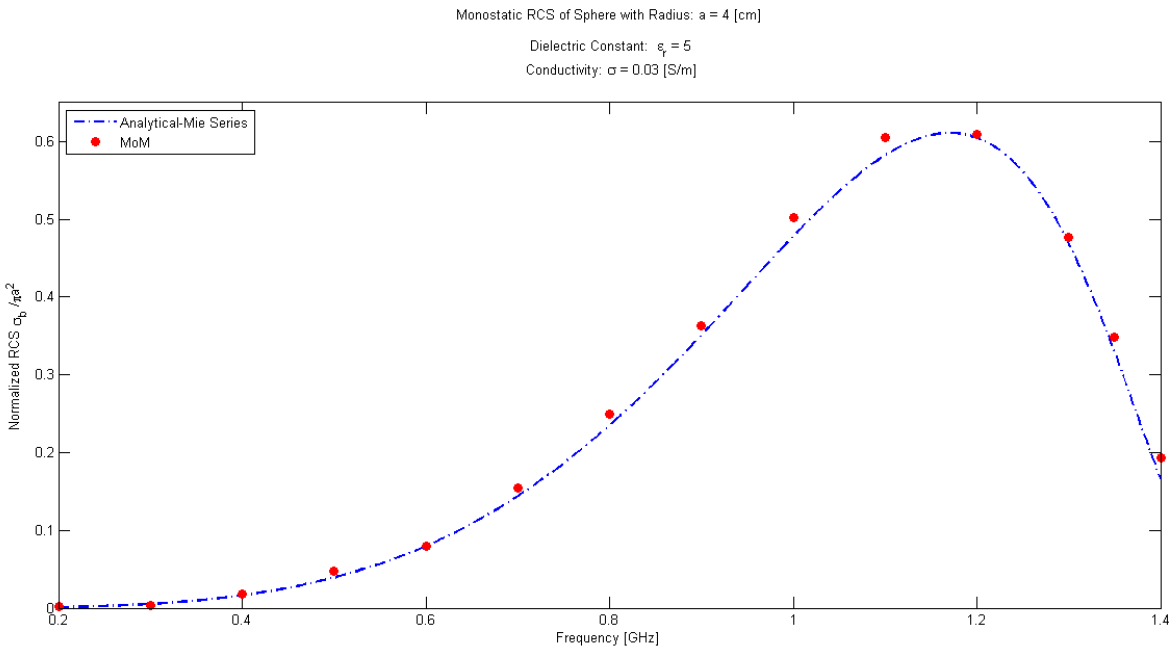

Figure 5.4 Analytical and Numerical monostatic RCS of dielectric sphere with radius $4\ cm$: $\varepsilon_r = 5$ and $\sigma = 0.03$ S/m. ($\theta_i = 0^0 \quad \varphi_i = 0^0$, $\theta_s = 180^0 \quad \varphi_s = 0^0$)

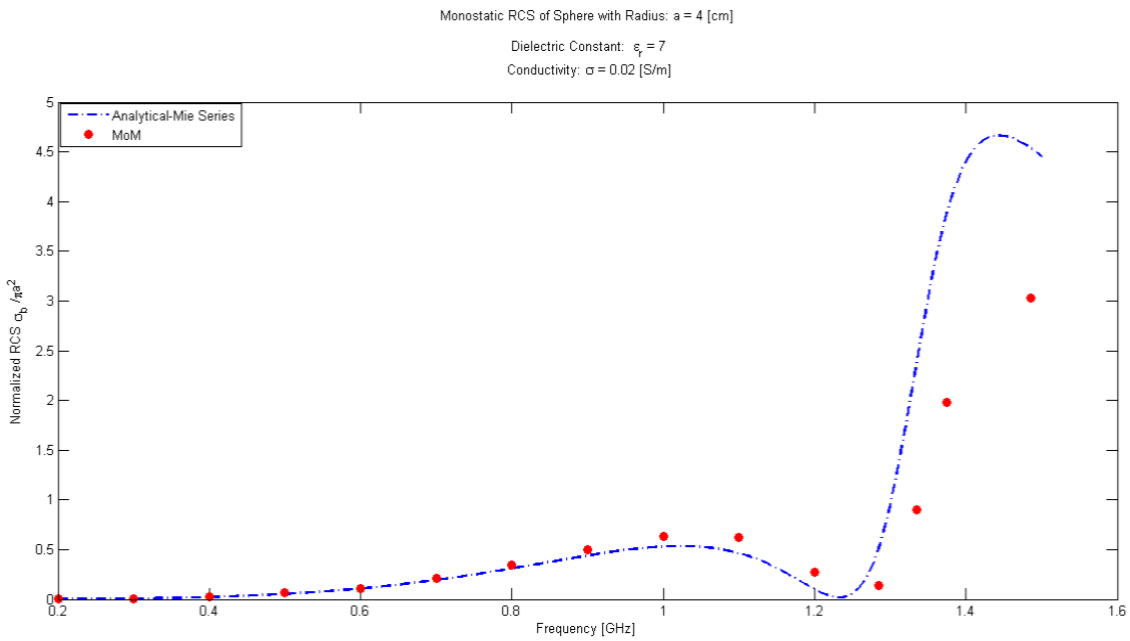

Figure 5.5 Analytical and Numerical monostatic RCS of dielectric sphere with radius $4\ cm$. $\varepsilon_r = 7$ and $\sigma = 0.02$ S/m.

These examples show the success of the MoM algorithm in Rayleigh scattering region. However, because of the insufficient discretization the results are not that good in Resonance and Optical scattering regions. Intelligent approaches, such as parallel computing and/or Matrix solvers are required in order to speed up the MoM algorithm and reduce memory.

Bi-static RCS of the lossy dielectric sphere is also calculated for the material values $\varepsilon_r = 5$ and $\sigma = 0.02$ S/m The example in Figure 5.6 shows bi-static RCS, co-polarized vertical case ($\sigma_{\theta\theta}$) for $0.6GHz$. Both analytical and numerical simulations are performed for 1^0 resolution (180 angles starting from $\theta = 0^0$ to $\theta = 180^0$).

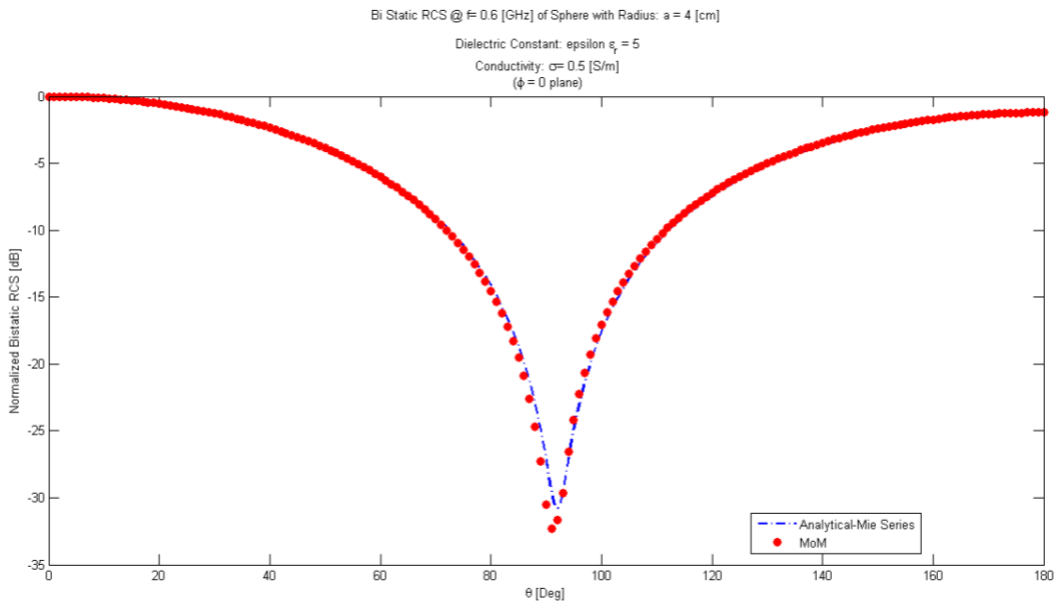

Figure 5.6 Bistatic angular RCS variation of a dielectric sphere at 0.6 GHz with radius $4\ cm$: $\varepsilon_r = 5$ and σ = 0.5 S/m.

The same sphere with the same dielectric constant and conductivity parameters are used in the next example given in Figure 5.7. Here, angular variation of bi-static RCS is shown for co-polarized vertical case $\sigma_{\theta\theta}$ in Mie region. The frequency is $1.4GHz$. As the frequency is increased, the complexity of the problem is also increased which gives rise to more required time to acquire the results. Hence, resolution of numerical cases is selected as 3^0 to reduce computational time. The big difference between numerical and analytical cases is around 100^0 which is less than $1dB$. For back scattering case, the difference is about $0.45dB$.

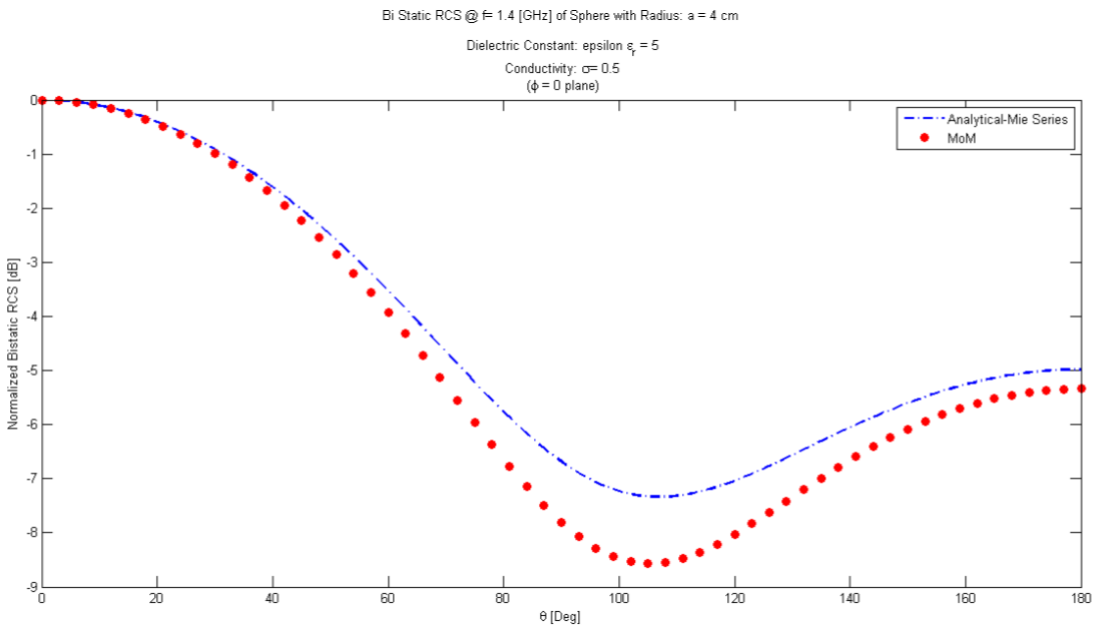

Figure 5.7 Bistatic angular RCS variation of a dielectric sphere at 1.4 GHz with radius $4\ cm$. $\varepsilon_r = 5$ and σ = 0.5 S/m.

The last example in Figure 5.8 belongs to the bi-static angular RCS variations for co-polarized horizontal case ($\sigma_{\varphi\varphi}$). Here, the frequency is $0.9GHz$ and constitutive parameters are selected as $\varepsilon_r = 4.5$ and σ = 0.05 S/m.

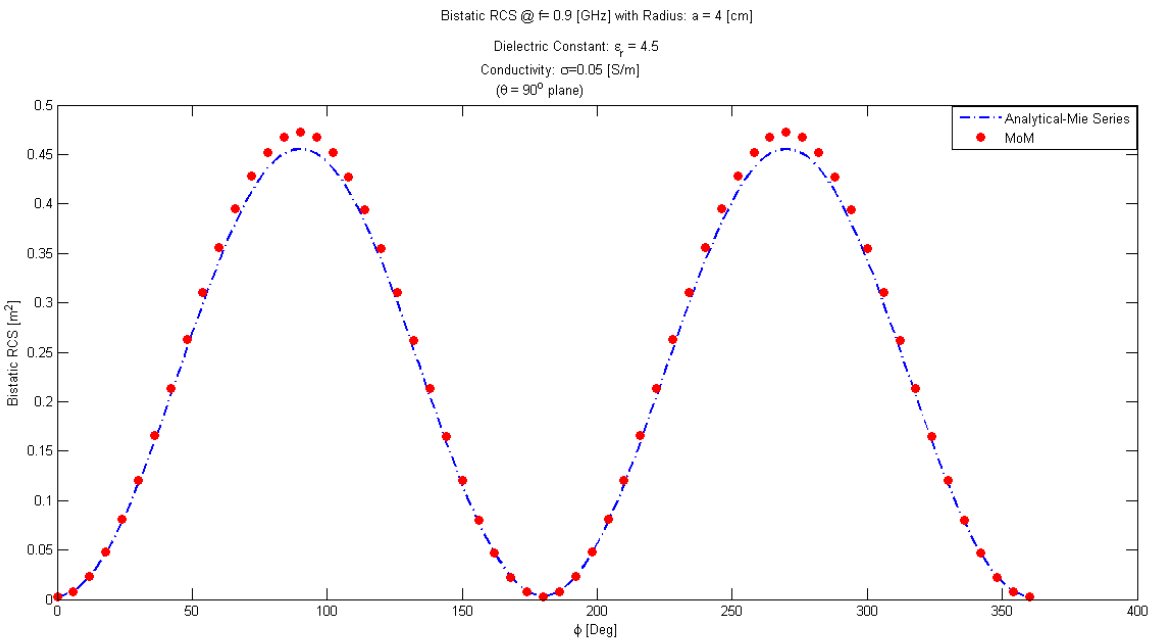

Figure 5.8 Bistatic angular RCS variation of a dielectric sphere at 0.9 GHzwith radius $4\ cm$. $\varepsilon_r = 4.5$ and σ = 0.5 S/m.

5.2 RCS Results for Canonical Structures

In the optical region, defined in 2nd section, commonly used high frequency asymptotic techniques (see [37], for details) are applied to RCS predictions. As the dimensions of the target are very large compared to radar wavelength, the techniques are used in this region only for investigation of some dominate parts of the targets such as reflecting planes, curvatures, edges, etc. Geometric Optics (GO) is one of them. Electromagnetic wave propagation is described in terms of rays by GO [29, 37]. GO RCS formulas of PEC plate dihedral and trihedral under the specified illuminations are given in Figure 5.9.

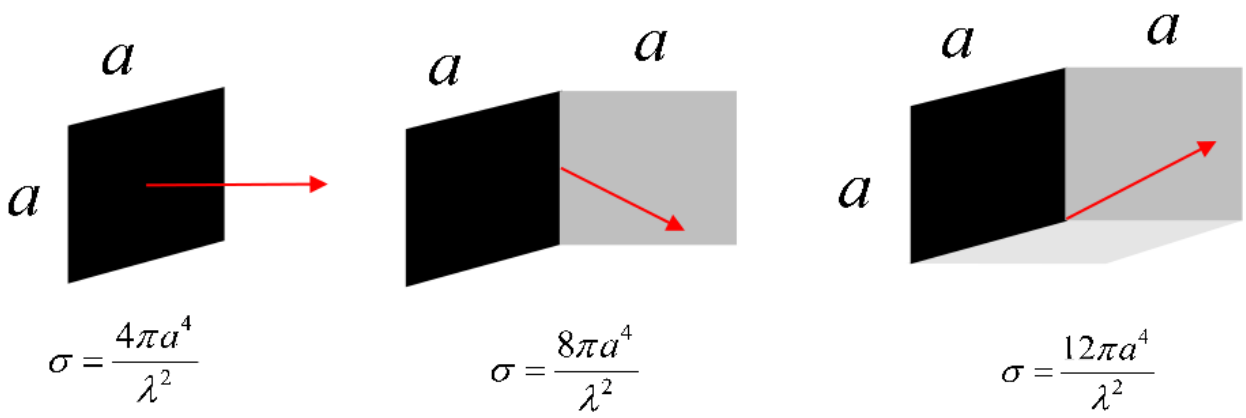

Figure 5.9 A PEC plate, a dihedral, and a trihedral, with an edge length of a. GO backscatter RCS formulas for the specified incident illumination.

In this section, RCS patterns of PEC layer trihedral examples are shown for different incident illumination angles. Simulations are done by performing both MoM algorithm and CST Microwave Studio, which applies Finite Difference Time Domain (FDTD) [38] technique to RCS prediction, simultaneously. Comparison of FDTD and MoM are given by following figures.

Figure 5.10 presents the angular Bi-static RCS patterns of a PEC layer. Edge length is determined as 2λ at $6GHz$. GO result is $-3dB$. Maximum RCS values are approximately at -3dB. Two plots in this figure belong to the MoM and FDTD. Figure 5.11 shows the results of PEC layer with different illumination angle.

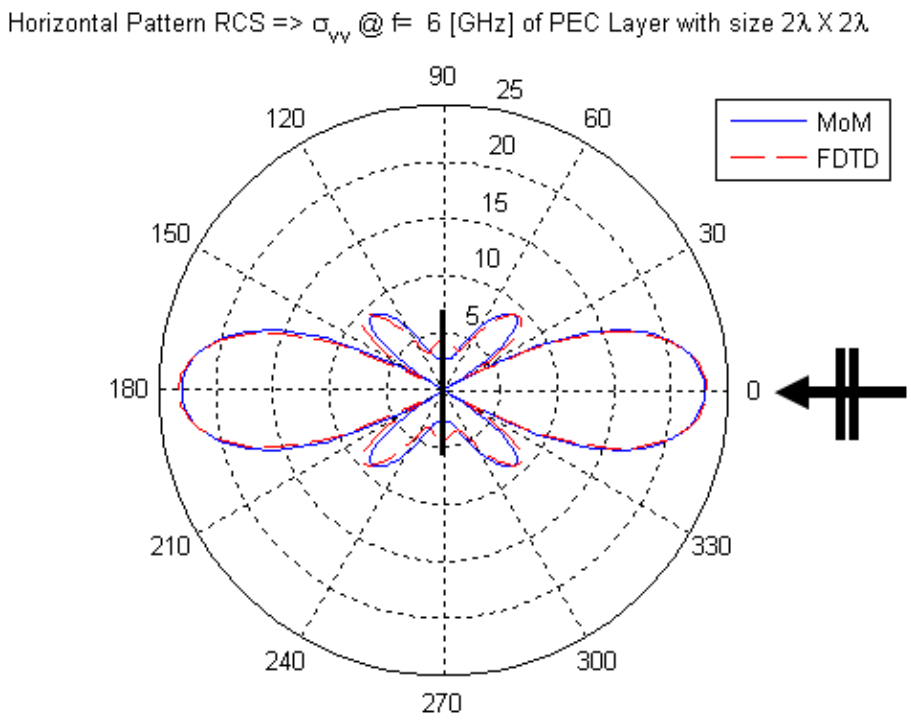

Figure 5.10 Normalized angular bistatic RCS patterns of a $10cm \times 10cm$ PEC square plate simulated in FDTD and MoM at $6\ GHz$. Maximum RCS values are approximately at -3dB. The angles of illumination are also pictured $\theta_i = 90^0 \ \ \varphi_i = 0^0$. The scattering angles were $\theta_s = 90^0\ 0^0 \le \varphi_s \le 360^0$.

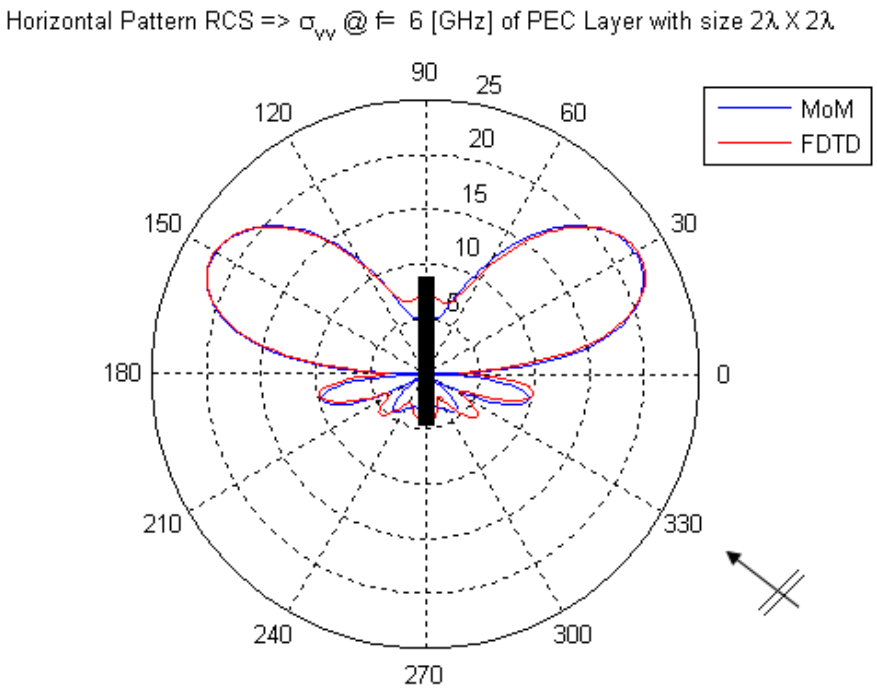

Figure 5.11 Normalized Angular bistatic RCS patterns of a $10cm \times 10cm$ PEC square plate simulated in FDTD and MoM at $6\ GHz$. Maximum RCS values are approximately at -3dB. The angles of illumination are also pictured $\theta_i = 90^0 \quad \varphi_i = 330^0$. The scattering angles were $\theta_s = 90^0\ 0^0 \le \varphi_s \le 360^0$

The example in Figure 5.12 shows bi static RCS pattern of a PEC trihedral. The size of object is $20\ cm$ (2 wavelength at $3\ GHz$) and is illuminated from 45^0.

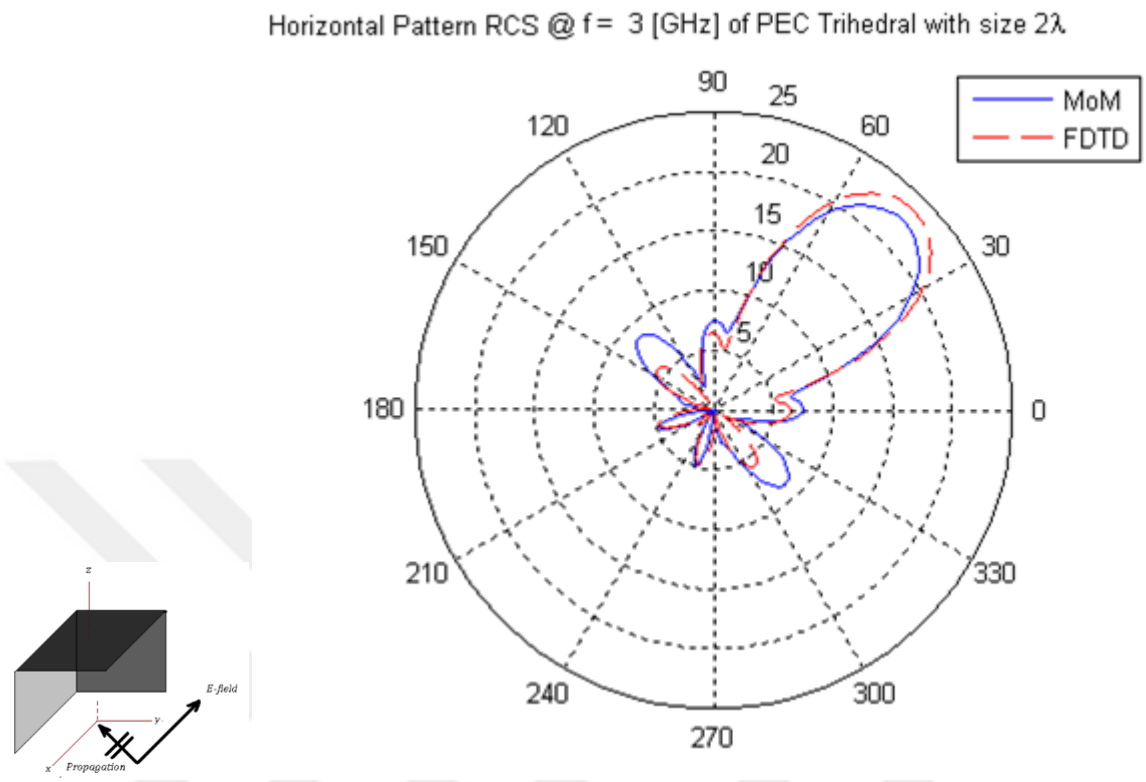

Figure 5.12 Normalized Angular bistatic RCS patterns of a $20\ cm$ PEC trihedral simulated in FDTD and MoM at $3\ GHz$. Maximum RCS values are approximately at -3dB. The angles of illumination is also pictured $\theta_i = 45^0$ $\varphi_i = 45^0$. The scattering angles were $\theta_s = 45^0$ $0^0 \le \varphi_s \le 360^0$

Figure 5.13 shows simulation results of a PEC object with arbitrary C-shaped geometry. Here, horizontal RCS pattern is shown. The simulations are done at 200 MHz. Maximum size of the object is $1.5\ m$(1 wavelength).

In these simulations of the canonical PEC structures, $\lambda_0 / 10$ discretization is sufficient to be able to acquire rough RCS results. Therefore, for PEC structures it gives an opportunity to observe canonical RCS results even in optical frequency region. The last two examples show bistatic RCS results for a PEC plate with size $5\lambda_0$ and $8\lambda_0$ for the frequencies 15 GHz and 24 GHz, respectively.

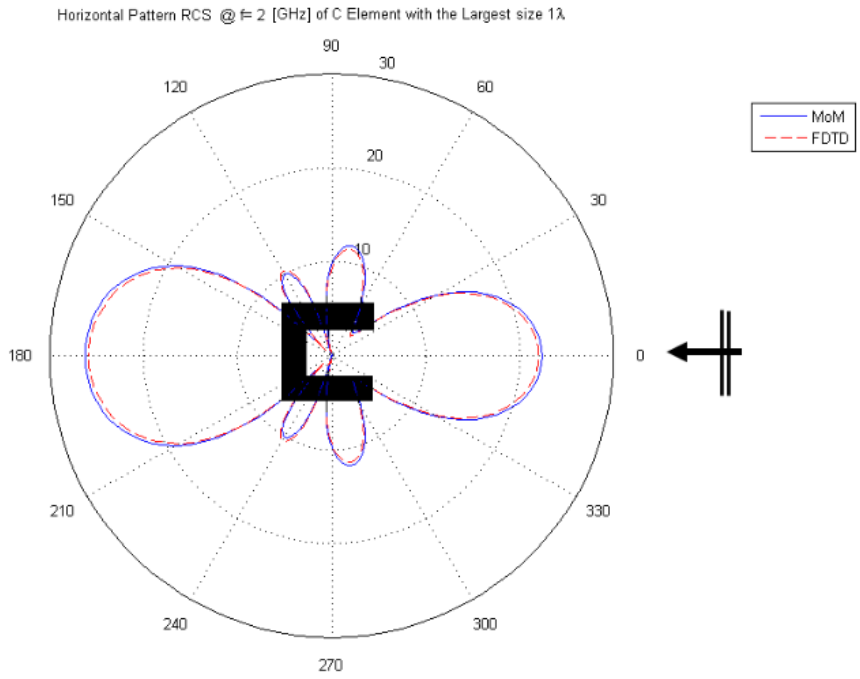

Figure 5.13 Normalized Angular bistatic RCS patterns of a $1.5\ m$ PEC C-Shaped element simulated in FDTD and MoM at $200\ MHz$. Maximum RCS values are approximately at 15.5dB. The angles of illumination are $\theta_i = 90^0$ $\varphi_i = 0^0$. The scattering angles were $\theta_s = 90^0$ $0^0 \le \varphi_s \le 360^0$

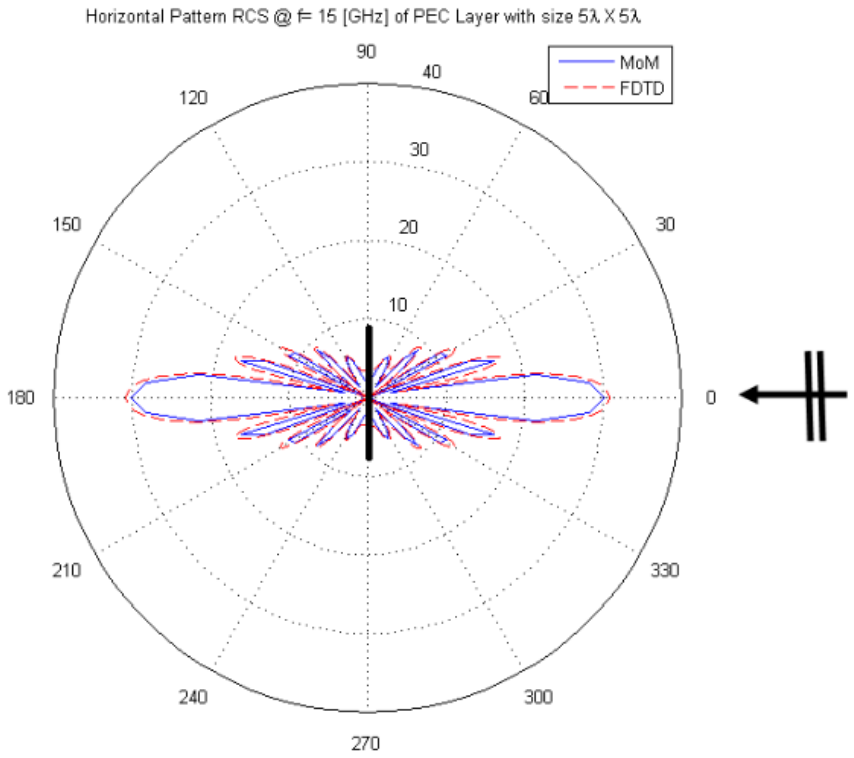

Figure 5.14 Normalized Angular bistatic RCS patterns of a $10cm \times 10cm$ PEC square plate simulated in FDTD and MoM at $15\ GHz$. The angles of illumination are also pictured $\theta_i = 90^0 \quad \varphi_i = 0^0$. The scattering angles were $\theta_s = 90^0\ 0^0 \le \varphi_s \le 360^0$.

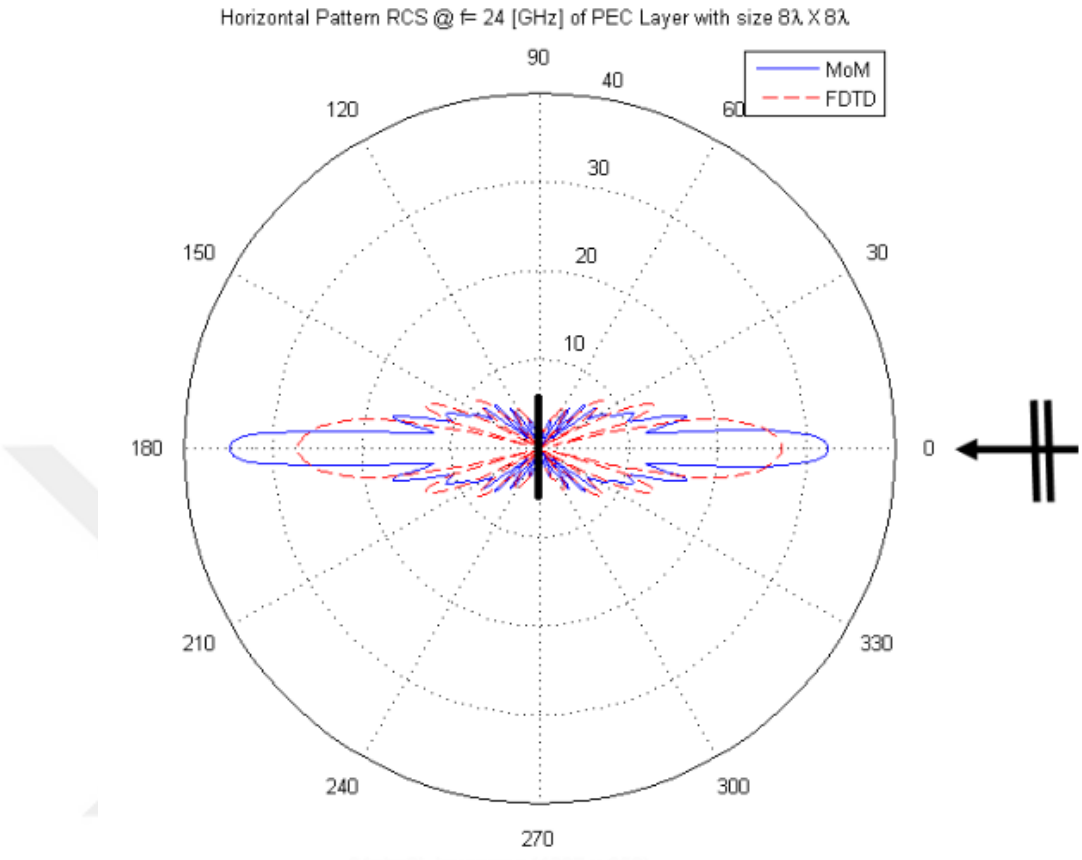

Figure 5.15 Normalized Angular bistatic RCS patterns of a $10cm \times 10cm$ PEC square plate simulated in FDTD and MoM at $24\ GHz$. The angles of illumination are also pictured $\theta_i = 90^0 \quad \varphi_i = 0^0$. The scattering angles were $\theta_s = 90^0\ 0^0 \le \varphi_s \le 360^0$.

6. CONCLUSION

A 3D MoM algorithm is developed in this thesis for the investigation of electromagnetic scattering from wave – object interaction. A MATLAB based program is written for implementation of the MoM algorithm. MoM requires vector Integral equations (VIE) and Dyadic Green's representation as the Kernel for arbitrary shapes and materials. In order to convert the VIE into a system of linear equations; the object is divided into cubic type cells where the required integration of dyadic Green's function do not converge if observation and source points are at the same cell. PV integration is applied to overcome the divergent problem of dyadic Green's function. Validation the numerical algorithm is done by comparing the results with analytical Mie solutions which solves the scattering problem for sphere.

The explanations about RCS definitions and criterions are given in Section 2. Polarization and criteria of frequency regions are also given in that part. The procedure of Mie Theory which is an analytical solution for scattering from spherical materials is handled in Section 3. Summary of the theory and short MATLAB scripts are given in this section to observe Mie scattering calculations.

Section 4 is reserved to analysis the linearization procedure of VIE and to attain sub-matrix elements of Dyadic Green's function. Whole procedure is done assuming that the 3-D object is a sphere. In the context of MoM, discretization was done by point matching technique. The volume of the sphere is discretized by cubical cells.

It is observed that to get accurate results for sphere with cubic model discretization, the cubical cells must much smaller than $\lambda/10$. Even the cells with $\lambda/150$ dimensions are applied in order to acquire more accurate results. This discretization increases the computational time and required memory. Hence, the monostatic bistatic RCS results only observed in the beginning of Mie

region. MoM algorithm is also applied to other simple canonical structures. It is observed that sufficient results are handled with $\lambda/10$ discretization of the cells. In order to obtain PEC structures it is possible to specify complex refractive index as $1000+1000i$ in MoM algorithm. For monostatic cases specifying conductivity parameter is more accurate. For PEC canonical structures, conductivity is determined as $\sigma = 10^5$. Given canonical examples are shown the bistatic RCS values for several angles of illumination. Commercial software, CST Microwave studio, is also used for numerical comparisons.

REFERENCES

[1] Mie, G., (1908), "Beigrade zur optik truber medien, speziell kolloidaler metallosungen", *Ann. Phys.*, 25, 377-455.

[2] Stratton, J. A., (1941), *Electromagnetic Theory*, New York: McGraw-Hill.

[3] Bohren C. F. and Huffman D. R., (1983), *Absorption and scattering of light by small particles*, New York: Wiley.

[4] King W. P. and Harrison C.W. (1971), "Scattering By Imperfectly Conducting Spheres", *IEEE Trans. Antennas Propagat.*, 19 (2), 197-207, March.

[5] Stephen J. J., (1961), "Radar Cross Section for Water And Ice Spheres", *J. Meteo.*, 18, 348-359, June.

[6] Sadiku M.N.O., (1985), "Refractive index of Snow at Microwave Frequencies", *Appl. Opt.*, 24 (4), 572-575, Feb.

[7] Wiscombe W. J., (1980), "Improved Mie Scattering Algorithms", *Appl. Opt.*, 19 (9), 1505-1509, May.

[8] Du H., (2014) "Mie Scattering Calculation", *Appl. Opt*., 43 (9), 1951-1956, March.

[9] Harrington R. F., (1993), *Field Computation by Moment Methods*, New York: Wiley-IEEE Press Series.

[10] Sadiku M. N. O., (2009), *Numerical Techniques in Electromagnetics with MATLAB*, New York: CRC Press.

[11] Balanis C.A., (1989), *Advanced Engineering Electromagnetics*, New York: John Wiley & Sons.

[12] Harrington R. F., (2001), *Time Harmonic Electromagnetic Fields*, New York: Wiley-IEEE Press Series.

[13] Andreasen M. G., (1964), "Scattering from parallel Metallic Cylinders with Arbitrary Cross Section", *IEEE Trans. Antennas Propagat.,* 12 (2), 746-754, Nov.

[14] Harrington R. F., (1969) "Radiation and Scattering from Bodies of Revolution", *J. Appl. Sci.,* 20 (1), 405-435, June.

[15] Govind S. and Wilton D. R., (1977), "Incorporation of Edge Conditions in Moment Method Solutions", *IEEE Trans. Antennas Propagat.,* 25 (6), 845-850, Nov.

[16] Rao S. M., Wilton D. R. and Glisson A. W., (1982), "Electromagnetic Scattering by Surfaces of Arbitrary shape", *IEEE Trans. Antennas Propagat.,* 30 (3), 409-417, May.

[17] Rao S. M., Sarkar T. K., Midya P. and Djordjevic A. R., (1991), "Electromagnetic radiation and scattering from finite conducting and dielectric structures: surface/surface formulation", *IEEE Trans. Antennas Propagat.,* 39 (7), 1034–1037, Jul.

[18] Van Bladel J., (1961), "Some Remarks on Green's Dyadic for Infinite Space", *IEEE Trans. Antennas Propagat.,* 9 (6), 563-566, Nov.

[19] Livesay D. E. and Chen K. M., (1974), "Electromagnetic Fields Induced Inside Arbitrarily Shaped Biological Bodies", *IEEE Trans. Microwave Theory. Tech.,* 22 (12), 1273-1280, Dec.

[20] C. C. Su, (1987), "A Simple Evaluation of Some Principle Value Integrals for Dyadic Green's Function Using Symmetry Property", *IEEE Trans. Antennas Propagat.,* 35 (3), 1306-1307, Nov.

[21] Hagmann M. J. and Levin R. L., (1987), "Criteria for Accurate usage of block models", *J. Microwave Power***,** 22, 19-27, Jan.

[22] D. H. Schaubert, D. R. Wilton and A. W. Glisson, (1984), "A Tetrahedral Modeling Method for Electromagnetic Scattering by Arbitrarily Shaped Inhomogeneous dielectric bodies", *IEEE Trans. Antennas Propagat.,* 32 (1), 77-85, Jan.

[23] J. J. H. Wang and J. R. Dubberley, (1989), "Computation of Fields in an Arbitrarily Shaped Heterogeneous Dielectric or Biological Body by an Iterative Conjugate Gradient Method", *IEEE Trans. Microwave Theory Tech.,* 37 (7), 1119-1125, Jul.

[24] Chew W. C., (1993), "The Use of Huygen's Equivalence Principle for Solving the Volume Integral Equation of Scattering", *IEEE Trans. Antennas Propagat.,* 41 (7), 897-904, Jul.

[25] Kottman J. P. and Martin O. J. F., (2000), "Accurate Solution of the Volume Integral Equation for High-Permittivity Scatterers", *IEEE Trans. Antennas Propagat.,* 48 (11), 1719-1726, Nov.

[26] Chew W.C., (2008), "A Novel Formulation of the Volume Integral Equation for General Large Electromagnetic Scattering Problems", *IEEE Antennas Propagat. Society International Symp.,* Jul. 5-11, San Diego, CA.

[27] Sevgi L. Uluışık Ç., Çakır G. and Çakır M., (2008), "RCS Modelling and Simulation, Part 1: A Tutorial Review of Definitions, Strategies and Canonical Examples", *IEEE Antennas Propagat. Magazine,* 50 (1), 115-126, Feb.

[28] Jay F., (1984), *IEEE Standard Dictionary of Electrical and Electronics Terms,* 3rd Ed., New York: John Wiley & Sons.

[29] Knott U. F., (1993), *Radar Cross Section Measurements,* New York: Van Nostrand Reinhold.

[30] Abramowitz M. and Stegun I. A. (1965), *Handbook* of *Mathematical Functions,* New York: Dover Publications Inc.

[31] Tai C. T., (1997), *Generalized Vector Dyadic Analysis,* 2nd Ed., New York: Wiley-IEEE Press.

[32] Felsen L. B. and Marcuvitz N., (1994), *Radiation and Scattering of Waves,* New York: John Wiley Sons Inc.

[33] Gao C., Verdin T. and Habashy T. M., (2005), "Analytical Techniques to Evaluate integrals of 3D and 2D Spatial Dyadic Green's Functions", *Progress in EM Research, PIER,* 52, 47-80.

[34] W. E. Byerly, (1983) *An Elementary Treatise On Fourier's Series and Spherical Cylindrical and Ellipsoidal Harmonics,* London: GINN & COMP.

[35] Born M. and Wolf E., (2003), *Principles of Optics,* 6th Ed., Cambridge: Cambridge Uni. Press.

[36] Ishimaru A., (1999), *Wave Propagation and Scattering in Random Media*, New York: Wiley-IEEE Press.

[37] Ufimtsev P. Y., (1996), "Comment on Diffraction Principles and Limitations of RCS Reduction Techniques", *Proc. IEEE,* 84 (12), 1830-1851, Dec.

[38] Sevgi L., (2014), *Electromagnetic Modeling and Simulation,* New York: Wiley-IEEE Press.

APPENDIX A:

EVALUATION OF THE DYADIC GREEN FUNCTION'S MATRIX ELEMENTS FOR SINGULAR CASE

The PV integral, defined in (4.11) can be expanded according to (4.15)

$$G_{x_p x_q}^{lk} = \left[\bar{\bar{I}} + \frac{1}{k_0^2} \nabla\nabla \right] \int_{V_k} g\left(\vec{r}_l, \vec{r}'\right) dv'. \tag{A.1}$$

As stated before, the scalar Green's function $g\left(\vec{r}_l, \vec{r}\right)$ is the impulse response of the scalar wave equation. From (4.9) one can obtain,

$$\int_{V_k} g\left(\vec{r}_l, \vec{r}'\right) dv' = -\frac{1}{k_0^2} \int_{V_k} \nabla^2 g\left(\vec{r}_l, \vec{r}'\right) dv' - \frac{1}{k_0^2} \int_{V_k} \delta\left(\vec{r}_l - \vec{r}'\right) dv'. \tag{A.2}$$

which reduces to:

$$\int_{V_k} \delta\left(\vec{r}_l - \vec{r}'\right) dv' = D\left(\vec{r}\right) = \begin{cases} 1 \; \vec{r}_l \in V_k \\ 0 \; \vec{r}_l \notin V_k \end{cases}. \tag{A.3}$$

Scalar Green's function satisfies $\nabla\left(g\left(\vec{r}_l - \vec{r}'\right)\right) = -\nabla'\left(g\left(\vec{r}_l - \vec{r}'\right)\right)$, where ∇' coordinates stands for derivative with respect to the source. Thus, (A.2) can be written as:

$$\int_{V_k} g\left(\vec{r}_l, \vec{r}'\right) dv' = \frac{1}{k_0^2} \nabla \cdot \int_{V_k} \nabla' g\left(\vec{r}_l, \vec{r}'\right) dv' - \frac{1}{k_0^2} \mathrm{D}\left(\vec{r}\right). \tag{A.4}$$

At this point, it is possible to apply alternative form of divergence theorem that states $\int_V \nabla\phi dv = \oiint_S \vec{e}_n \phi ds$, where ϕ is an arbitrary scalar function [2] (A.4) becomes,

$$\int_{V_k} g\left(\vec{r}_l, \vec{r}'\right) dv' = \frac{1}{k_0^2} \nabla \cdot \oiint_{S_k} \vec{e}_n g\left(\vec{r}_l, \vec{r}'\right) ds' - \frac{1}{k_0^2} D\left(\vec{r}\right), \tag{A.5}$$

where S_k is the closed surface of the integration volume V_k and $\vec{e}_n$ is the outward unit normal vector of the surface boundary S_k. Gradient of a scalar function gives a vector; gradient of a vector results a dyadic. Therefore, integral of scalar Green's function over the volume V_k is a scalar function; gradient of gradient of it gives a dyadic tensor. To be able to find an appropriate result for $\nabla\nabla\int_{V_k} g\left(\vec{r}_l,\vec{r}'\right)dv'$, one can apply the theorem stated above to (A.1) and obtain

$$\nabla\nabla\int_{V_k} g\left(\vec{r}_l,\vec{r}'\right)dv' = -\nabla\int_{V_k}\nabla' g\left(\vec{r}_l,\vec{r}'\right)dv' = -\nabla\oint_{S_k}\vec{e}_n g\left(\vec{r}_l,\vec{r}'\right)ds'. \tag{A.6}$$

Combining (A.1), (B.5) and (B.6) yields

$$\bar{\bar{G}}_{pq}^{lk} = \frac{1}{k_0^2}\left[\bar{\bar{I}}\left(\nabla\cdot\oint_{S_k}\vec{e}_n g\left(\vec{r}_l,\vec{r}'\right)ds' - D\left(\vec{r}\right)\right) - \nabla\oint_{S_k}\vec{e}_n g\left(\vec{r}_l,\vec{r}'\right)ds'\right]. \tag{A.7}$$

In this form, integration of the volume is reduced to the surface integral. The small volumes are handled as cubic volumes, and the integral of a cubic volume will be found by summation of flux through six surfaces of the cube. According to that (A.7) can be written as

$$\bar{\bar{G}}_{pq}^{lk}\left(\vec{r}\right) = \frac{1}{k_0^2}\begin{bmatrix}\bar{\bar{I}}\nabla\cdot\left(\vec{e}_x\left(S_x^{k+}-S_x^{k-}\right)+\vec{e}_y\left(S_y^{k+}-S_y^{k-}\right)+\vec{e}_z\left(S_z^{k+}-S_z^{k-}\right)\right)-\bar{\bar{I}}D\left(\vec{r}\right)-\ldots \\ \ldots\nabla\left(\vec{e}_x\left(S_x^{k+}-S_x^{k-}\right)+\vec{e}_y\left(S_y^{k+}-S_y^{k-}\right)+\vec{e}_z\left(S_z^{k+}-S_z^{k-}\right)\right)\end{bmatrix}. \tag{A.8}$$

Suppose that in Cartesian coordinate system, the small volume V_k is in cubic form, which has a center located at $\left(x_c^k, y_c^k, z_c^k\right)$ and the side length of the cell is $2a$ as shown in Figure A.1. The observation point is located at an arbitrary l^{th} cell with coordinates $\left(x_l, y_l, z_l\right)$. The scalar Green's function, $g\left(\vec{r}_l,\vec{r}'\right)$, in Cartesian coordinate system is:

$$g\left(\vec{r}_l,\vec{r}'\right)=\frac{\mathrm{e}^{ik_0\sqrt{\left(x_l-x'\right)^2+\left(y_l-y'\right)^2+\left(z_l-z'\right)^2}}}{4\pi\sqrt{\left(x_l-x'\right)^2+\left(y_l-y'\right)^2+\left(z_l-z'\right)^2}}. \tag{A.9}$$

The flux through the six faces of the cube will be:

$$\vec{e}_{x_n}S_{x_n}^{k+}=\vec{e}_{x_n}\int_{x_{pc}^k-a}^{x_{pc}^k+a}\int_{x_{qc}^k-a}^{x_{qc}^k+a}\left[g\left(\vec{r}_l,r'\right)\Big|_{x_n'=x_{n_c}^k+a}\right]dx_q dx_p, \tag{A.10a}$$

$$\vec{e}_{x_n}S_{x_n}^{k-}=-\vec{e}_{x_n}\int_{x_{pc}^k-a}^{x_{pc}^k+a}\int_{x_{qc}^k-a}^{x_{qc}^k+a}\left[g\left(\vec{r}_l,r'\right)\Big|_{x_n'=x_{n_c}^k-a}\right]dx_q dx_p,$$

$$x=x_1,\ \ y=x_2,\ \ z=x_3,$$
$$n,p,q=1,2,3,$$
$$n\neq p\neq q. \tag{A.10b}$$

In addition, (A.10a) and (A.10b) can be generalized as

$$g\left(\vec{r}_l,r'\right)\Big|_{x_n'=x_{n_c}^k\pm a}=\frac{e^{ik_0R_{x_n}^{\pm}}}{4\pi R_{x_n}^{\pm}},$$
$$R_{x_n}^{\pm}=\sqrt{\left(x_{n_l}-\left(x_{n_c}^k\pm a\right)\right)^2+\left(x_{p_l}-x_p{}'\right)^2+\left(x_{q_l}-x_q{}'\right)^2},$$
$$\vec{e}_{x_n}S_{x_n}^{k}=\vec{e}_{x_n}\left(S_{x_n}^{k+}-S_{x_n}^{k-}\right)=\vec{e}_{x_n}\frac{1}{4\pi}\int_{x_{pc}^k-a}^{x_{pc}^k+a}\int_{x_{qc}^k-a}^{x_{qc}^k+a}\left[\frac{e^{ik_0R_{x_n}^{+}}}{R_{x_n}^{+}}-\frac{e^{ik_0R_{x_n}^{-}}}{R_{x_n}^{-}}\right]dx_q dx_p, \tag{A.11}$$
$$x=x_1,\ \ y=x_2,\ \ z=x_3,$$
$$n,p,q=1,2,3,$$
$$n\neq p\neq q.$$

The gradient of the flux, $\vec{e}_{x_n}S_{x_n}^{k}$,defined in (A.11), can be generalized explicitly as

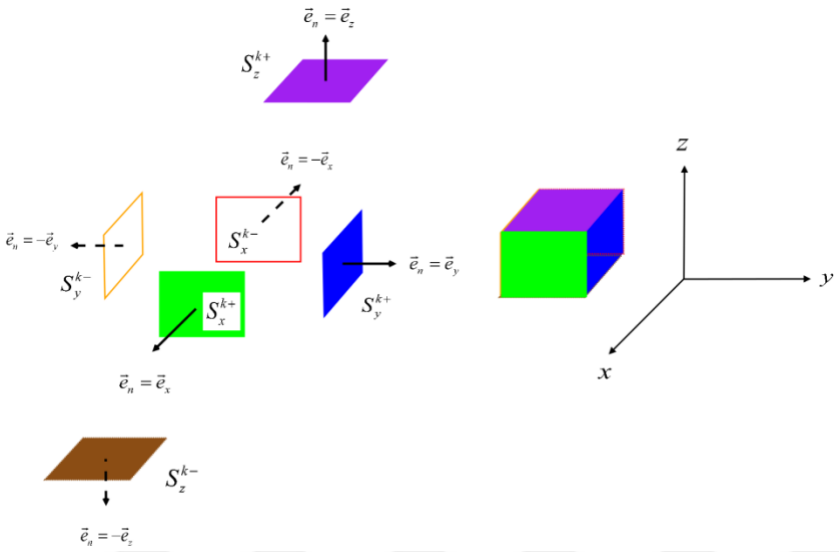

Figure A.1: The flux integrals for six sides of the cube and the outward normal vectors for each side.

$$\nabla\left(\vec{e}_{x_n} S^k_{x_n}\right) = \vec{e}_{x_n}\vec{e}_{x_n}\partial S^k_{x_n x_n} + \vec{e}_{x_p}\vec{e}_{x_n}\partial S^k_{x_n x_p}$$
$$= \vec{e}_x\vec{e}_x\partial S^k_{xx} + \vec{e}_x\vec{e}_y\partial S^k_{xy} + \vec{e}_x\vec{e}_z\partial S^k_{xz} + \vec{e}_y\vec{e}_x\partial S^k_{yx} + \vec{e}_y\vec{e}_y\partial S^k_{yy} + \vec{e}_y\vec{e}_z\partial S^k_{yz} + \vec{e}_z\vec{e}_x\partial S^k_{zx} + \vec{e}_z\vec{e}_y\partial S^k_{zy} + \vec{e}_z\vec{e}_z\partial S^k_{zz}. \quad \text{(A.12)}$$

Combining (A.1) and (A.12) one can obtain

$$\bar{\bar{G}}^{lk}_{pq} = \frac{1}{k_0^2}\begin{Bmatrix} \bar{\bar{I}}\left(-D(\vec{r}) + \partial S^k_{xx} + \partial S^k_{yy} + \partial S^k_{zz}\right)... \\ -\vec{e}_x\vec{e}_x\partial S^k_{xx} - \vec{e}_x\vec{e}_y\partial S^k_{xy} - \vec{e}_x\vec{e}_z\partial S^k_{xz}... \\ -\vec{e}_y\vec{e}_x\partial S^k_{yx} - \vec{e}_y\vec{e}_y\partial S^k_{yy} - \vec{e}_y\vec{e}_z\partial S^k_{yz}... \\ -\vec{e}_z\vec{e}_x\partial S^k_{zx} - \vec{e}_z\vec{e}_y\partial S^k_{zy} - \vec{e}_z\vec{e}_z\partial S^k_{zz} \end{Bmatrix}. \quad \text{(A.13)}$$

Expanding (A.13) for non-diagonal elements yields

$$\partial S^k_{x_p x_n} = \frac{\partial}{\partial x_{p_l}}\left(S^{k+}_{x_n} - S^{k-}_{x_n}\right),$$
$$= \frac{1}{4\pi}\int_{x^k_{p_c}-a}^{x^k_{p_c}+a}\int_{x^k_{q_c}-a}^{x^k_{q_c}+a}\left(x_{p_l} - x_p{}'\right)\left[\frac{e^{ik_0R^+_{x_n}}\left(ik_0R^+_{x_n} - 1\right)}{\left(R^+_{x_n}\right)^3} - \frac{e^{ik_0R^-_{x_n}}\left(ik_0R^-_{x_n} - 1\right)}{\left(R^-_{x_n}\right)^3}\right]dx_q dx_p,$$
$$x = x_1,\ \ y = x_2,\ \ z = x_3, \quad \text{(A.14)}$$
$$n, p, q = 1, 2, 3,$$
$$n \neq p \neq q.$$

Also for diagonal elements it is obtained as

$$\partial S^{k}_{x_n x_n} = \frac{\partial}{\partial x_{n_l}}\left(S^{k+}_{x_n} - S^{k-}_{x_n}\right)$$

$$= \frac{1}{4\pi}\int_{x^k_{p_c}-a}^{x^k_{p_c}+a}\int_{x^k_{q_c}-a}^{x^k_{q_c}+a}\left[\frac{\left(x_{n_l}-x_{n_c}-a\right)e^{ik_0R^+_{x_n}}\left(ik_0R^+_{x_n}-1\right)}{\left(R^+_{x_n}\right)^3}\cdots - \frac{\left(x_{n_l}-x_{n_c}+a\right)e^{ik_0R^-_{x_n}}\left(ik_0R^-_{x_n}-1\right)}{\left(R^-_{x_n}\right)^3}\right]dx_q dx_p,$$

$$x = x_1,\quad y = x_2,\quad z = x_3, \qquad \text{(A.15)}$$

$$n, p, q = 1, 2, 3,$$

$$n \neq p \neq q.$$

After defining the surface integrals, (A.13) in matrix form equals to:

$$\bar{\bar{G}}^{lk}_{pq} = \begin{bmatrix} -D\left(\vec{r}\right)+\partial S^k_{yy}+\partial S^k_{zz} & -\partial S^k_{xy} & -\partial S^k_{xz} \\ -\partial S^k_{yx} & -D\left(\vec{r}\right)+\partial S^k_{xx}+\partial S^k_{zz} & -\partial S^k_{yz} \\ -\partial S^k_{zx} & -\partial S^k_{zy} & -D\left(\vec{r}\right)+\partial S^k_{xx}+\partial S^k_{yy} \end{bmatrix}. \qquad \text{(A.16)}$$

Due to the definition of the gradient of the flux given in (A.14) and (A.15) it is obvious that the matrix, defined in (A.16) is a symmetric matrix

$$\begin{aligned} \partial S^k_{xy} &= \partial S^k_{yx}, \\ \partial S^k_{xz} &= \partial S^k_{zx}, \\ \partial S^k_{yz} &= \partial S^k_{zy}. \end{aligned} \qquad \text{(A.17)}$$

The explicit expression of $\bar{\bar{G}}^{lk}_{pq}$ given in (A.16) and the definition of flux integral and its derivatives acquired in (A.11), (A.14), and (A.15) are valid for any arbitrary selected observation point locations. However, when the singular case is considered, the observation and the source

point are on the same cell $\left(\vec{r}_l = \vec{r}'\right)$. According to that the distance between observation and source vectors, $R^+_{x_n}$ & $R^-_{x_n}$ defined in (A.11), become

$$R^+_{x_n} = R^-_{x_n} = a. \tag{A.18}$$

Thus, according to (A.14), the non-diagonal elements of (A.16) become

$$\partial S^k_{xy} = \partial S^k_{yz} = \partial S^k_{xz} = 0. \tag{A.19}$$

Therefore, the singular k^{th} cell, one can obtain

$$\begin{aligned}
&\bar{\bar{G}}^{kk}_{nn} = \left(-D\left(\vec{r}\right) + \partial S^k_{pp} + \partial S^k_{qq}\right)\bar{\bar{I}};\\
&\bar{\bar{G}}^{kk}_{nn} = \begin{bmatrix} -D\left(\vec{r}\right) + \partial S^k_{yy} + \partial S^k_{zz} & 0 & 0 \\ 0 & -D\left(\vec{r}\right) + \partial S^k_{xx} + \partial S^k_{zz} & 0 \\ 0 & 0 & -D\left(\vec{r}\right) + \partial S^k_{xx} + \partial S^k_{yy} \end{bmatrix},\\
&x = x_1,\ \ y = x_2,\ \ z = x_3,\\
&n, p, q = 1, 2, 3,\\
&n \neq p \neq q.
\end{aligned} \tag{A.20}$$

As shown in Figure B.2 the cubic cell will be approximated by equivalent spherical cells. The side length of cubic cell is determined as $2a$ therefore the radius of equivalent spherical cell will be $a_{eq} = \left(3/4\pi\right)^{1/3} 2a$.

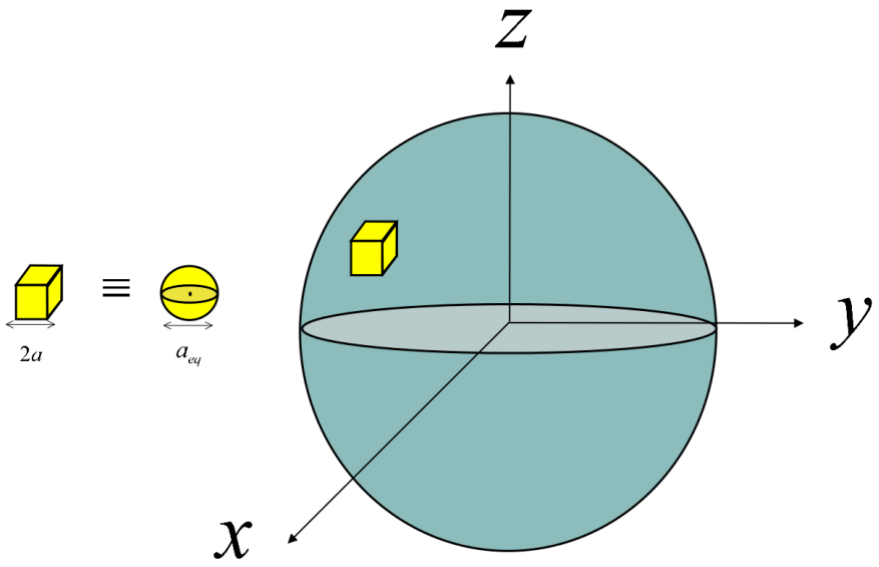

Figure B.2: The cubic cell on the sphere and the equivalent spherical cell

Because of the symmetry, the following relation exists for $\partial S_{xx}^k, \partial S_{yy}^k, \partial S_{zz}^k$:

$$\partial S_{xx}^k = \partial S_{yy}^k = \partial S_{zz}^k. \tag{A.21}$$

Furthermore, due to (A.7) and (A.20),

$$\partial S_{xx}^k + \partial S_{yy}^k + \partial S_{zz}^k = -\iint_{S_k} \nabla' \cdot \vec{e}_n g\left(\vec{r}_l, \vec{r}'\right) ds'. \tag{A.22}$$

Combination of (A.21) and (A.22) leads

$$\partial S_{xx}^k = \partial S_{yy}^k = \partial S_{zz}^k = -\frac{1}{3}\iint_{S_k} \nabla' \cdot \vec{e}_n g\left(\vec{r}_l, \vec{r}'\right) ds' = -\frac{1}{3}\int_0^{2\pi}\int_0^{\pi} \frac{\partial}{\partial r'}\left(g\left(\vec{r}_l, \vec{r}'\right)\right) \mathrm{r}'^2 \sin\theta' d\theta' d\varphi',$$

(A.23)

where outward unit normal $\vec{e}_n$ is on $\vec{r}'$-direction which can be defined in terms of Cartesian coordinates as

$$\vec{e}_{r'} = \vec{e}_x \sin\theta' \cos\varphi' + \vec{e}_y \sin\theta' \sin\varphi' + \vec{e}_z \cos\theta'. \tag{A.24}$$

The $g\left(\vec{r}_l,\vec{r}'\right)$ is a function of $\left|\vec{r}_l-\vec{r}'\right|$, therefore, it is possible to define a spherical coordinate system centered at $\vec{r}_l$. Without loss of generality it is possible to set $\vec{r}_l=0$. Then it follows that

$$g\left(\vec{r}_l,\vec{r}'\right)\Big|_{\vec{r}_l=0}=g\left(r'\right)=\frac{e^{ik_0r'}}{4\pi r'}. \tag{A.25}$$

And the derivative of $g\left(r'\right)$ with respect to r' is equal to

$$\frac{\partial}{\partial r'}\left(g\left(r'\right)\right)=\frac{\left(ik_0r'-1\right)e^{ik_0r'}}{4\pi r'^2}. \tag{A.26}$$

Using (A.25) and (A.26) in (A.23) yields

$$\partial S_{xx}^k=\partial S_{yy}^k=\partial S_{yy}^k=\frac{1}{3}\left(1-ik_0a_{eq}\right)e^{ik_0a_{eq}}. \tag{A.27}$$

Substituting (A.27) into (A.20) yields result for the k^{th} singular cell

$$G_{pq}^{kk}=\frac{1}{3k_0^2}\left[2\left(1-ik_0a_{eq}\right)e^{ik_0a_{eq}}-3\right]\bar{\bar{I}}=\delta_{pq}\left\{\frac{1}{3k_0^2}\left[2\left(1-ik_0a_{eq}\right)e^{ik_0a_{eq}}-3\right]\right\}. \tag{A.28}$$

CURRICULUM VITAE

Name Surname **:** Ahmet SEFER

Place and Date of Birth: ******** / **********

Address **:**

E-Mail **:**

B.Sc. **:** Bilkent University, Engineering Department, Electrical and Electronics Engineering Program.